SEIB–DGVM: A New Dynamic Global Vegetation Model using a Spatially Explicit Individual-Based Approach

Hisashi SATO[1], Akihiko ITOH[1, 2], and Takashi KOHYAMA[1, 3]

[1] Frontier Research Center for Global Change (FRCGC), Japan Agency for Marine-Earth Science and Technology (JAMSTEC), 3173-25 Showamachi, Kanazawa-ku, Yokohama-City, Kanagawa 236-0001, JAPAN

[2] National Institute for Environmental Studies, 16-2 Onogawa, Tsukuba-City, Ibaraki 305-8506, JAPAN

[3] Graduate School of Environmental Earth Science, Hokkaido University, Kita10-Nishi5, Kita-ku, Sapporo-City, Hokkaido 060-0810, JAPAN

[1] Corresponding author: hsato@jamstec.go.jp; fax: +81-45-778-5497

Key words: dynamic global vegetation model, biogeochemical model, individual-base model, plant community-dynamics, size structure, vegetation dynamics

Date of receipt:

Abstract

We report the development of a new Spatially Explicit Individual-Based Dynamic Global Vegetation Model (SEIB–DGVM), the first DGVM that can simulate the local interactions among individual trees within a spatially explicit virtual forest. In the model, a sample plot is placed at each grid box, and then the growth, competition, and decay of each individual tree within each plot is calculated by considering the environmental conditions for that tree as it relates to the trees that surround it. Based on these parameters only, the model simulated time lags between climate change and vegetation change. This time lags elongated when original biome was forest, because existing trees prevent newly establish trees from receiving enough sunlight and space to quickly replace the original vegetation. This time lags also elongated when horizontal heterogeneity of sunlight distribution was ignored, indicating the potential importance of horizontal heterogeneity for predicting transitional behavior of vegetation under changing climate. On a local scale, the model reproduced climate zone-specific patterns of succession, carbon dynamics, and water flux, although on a global scale, simulations were not always in agreement with observations. Because the SEIB–DGVM was formulated to the scale at which field biologists work, the measurements of relevant parameters and data comparisons are relatively straightforward, and the model should enable more robust modeling of terrestrial ecosystems.

Text

Introduction

Climatic conditions affect terrestrial ecosystems, but terrestrial ecosystems also affect the climate, particularly through evapotranspiration, the carbon cycle, and albedo (Foley et al., 2003). The degree, the sign (negative or positive), and the geographical distribution of vegetation feedbacks on climate all play a role in determining the climatic condition and the local distribution and functioning of terrestrial ecosystems. Many biogeochemical models have been developed, some of them combined with General Circulation Models (e.g. Woodward et al., 1998; Cox et al., 2000; Joos et al., 2001), to simulate the effects of global climate change on terrestrial ecosystems (Peng, 2000; Arora, 2002).

These biogeochemical models have taken either a static (time-independent) approach or a dynamic (time-dependent) approach. Static biogeochemical models (e.g. Neilson, 1995; Woodward et al., 1995; Haxeltine and Prentice, 1996) simulate plant physiological processes (e.g. photosynthesis, respiration, and growth) under a static set of climatic conditions, altering the distribution of vegetation types using criteria that maximize the leaf area index (LAI) or net primary production (NPP). These models do not factor in time when simulating changes in vegetation, even though there may be hundreds or thousands of years between climate change and vegetation change (Kohyama and Shigesada, 1995; Kohyama, 2005; Takenaka, 2005). Forecasts of rapid climate change during the next 100–200 years, fueled by an increase in greenhouse gases, have motivated the development of models that predict the transient behavior of terrestrial ecosystems.

To enable the simulation of transient changes in vegetation distribution and function, static biogeographical models have been expanded into 'dynamic' models by introducing plant dynamic modules, which include factors such as establishment, competition, mortality, and disturbance (Cramer et al., 2001). The majority of such Dynamic Global Vegetation Models (DGVMs; e.g., Friend et al., 1997; Kucharik et al., 2000; Cox, 2001; Sitch et al., 2003; Woodward and Lomas, 2004; Krinner et al., 2005) represent plant dynamics as competitive changes of foliar-projective-cover of each plant functional type (PFT) to conserve number of driving parameters and computer power. This approach is based on an assumption that plant competition occurs among PFTs, which is represented by average individuals. However, in reality, plant competitions occurs locally among heterogeneous individuals, because plant resources (light, water, nutrient, and space) are locally distributed. Such individual-based spatially explicit dynamics have already been adopted and verified in a gap model SORTIE (Pacala and Deutschman, 1995), suggesting that these types of interactions play a central role in ecosystem succession and production. In biogeochemical models, Hybrid3 (Friend et al. 1997) and LPJ–GUESS (Smith et al., 2001) adopted individual based approach. These models assume horizontally homogeneous patches, and simulate the growth of individual trees on a number of the replicate patches. However, horizontally homogeneous patch would make unrealistic perturbation of forest environment. For example, when a patch size is relatively small, a death of canopy tree would induce larger changes of light environment for these horizontal homogeneous patch models than for actual forest, where a significant amount of shading occur from the surrounding patches.

We have developed a new dynamic biogeochemical model called the SEIB–DGVM (Spatially Explicit Individual-Based Dynamic Global Vegetation Model). As far as authors know, this is

the first biogeochamical model with 3-dimentional representaion of forest structure, where individual trees compete for light and space. This representation of plant dynamics should have advantages over previous individual based biogeochemical models. First, observations of forest structure and dynamics can be directly used as tuning or validation data, without introducing additional assumptions. Second, it enables to calculate sunlight distribution among individuals more properly, and thus expected to have more accurate representation of plant competition. In this paper, we will present how this representation forest structure affects the transient behavior of vegetation along climatic change.

Model description

Overview

The simulation unit of the SEIB–DGVM is a 30 × 30-m spatially explicit virtual forest, in which individual trees establish, compete, and die. A grass layer also exists in the forest under the tree canopy. Appendix B1 shows the input and output of the model. Appendix B2 summarizes the processes represented, which can be classified into three groups: physical, physiological, and vegetation dynamics. The SEIB–DGVM utilizes three computational time steps: a daily time step for all physical and physiological processes except for soil decomposition and tree growth, a monthly time step for soil decomposition and tree growth, and an annual time step for vegetation dynamics and disturbance. Appendix B3 lists the symbols used in the model's equations. Those that begin with a capital letter are constants, while those that begin with a lowercase letter are variables. Plant species are classified into 10 plant functional types (PFTs) to enable global-scale simulation (Table 1; Sitch et al., 2003).

These PFTs can coexist in the same simulation plot. Program code and forcing data used in this manuscript are available on internet (sato.jfast1.net/seib).

The main objective of this paper is to examine possibility that spatially explicit individual-based treatment of forest structure has important roles in biogeochemical model. This approach accompanies increments of interactive mechanisms in simulations. Hence, to avoid risks of unknowability for the cause of simulation output, we tried to construct the model not to be over complicated, while biogeochemical model framework maintains. Taking the example of photosynthetic model, we employed empirical based model instead of the Farquhar's scheme (Farquhar and Caemmerer, 1982; Farquhar et al., 1980). The Farquhar's scheme is almost universally adopted by other DGVMs, but its behavior is not easy to predict from its formulation. Climatic data for driving simulation was also simplified by averaging interannual variability.

Plant properties

Woody PFTs are represented by individual trees composed of three organs: the crown and the trunk, both of which are cylindrical, and the fine roots, which are formless (Fig. 1). The crown is defined by biomass ($mass_{leaf}$), leaf area (la), diameter ($crown_{diameter}$), and depth ($crown_{depth}$); the trunk, by biomass ($mass_{trunk}$), height ($height$), and the diameters of sapwood ($dbh_{sapwood}$) and heartwood ($dbh_{heartwood}$); the fine roots, by biomass ($mass_{root}$) only. Trunk biomass ($mass_{trunk}$) includes both branch and coarse root biomass. Besides these variables, each individual tree has a reserve resource ($mass_{stock}$), which is used for foliation after the dormant phase (for deciduous PFTs) and after fires. Grass PFTs are represented in a much simpler way, consisting of leaf, root, and a reserve resource, all of which are represented by biomass per

unit area ($gmass_{leaf}$, $gmass_{root}$, and $gmass_{stock}$, respectively).

Carbon cycles

Figure 2 provides an overview of the carbon cycle as represented in the SEIB–DGVM. Atmospheric CO_2 is assimilated by the foliage of woody PFTs and grass PFTs. This assimilated carbon is then transferred to all of the other organs, where maintenance and growth respiration occurs. All respired carbon is recycled to the atmosphere as CO_2. At the same time, defoliation at the end of the growing season, turnover of leaves and fine roots, and tree death produce litter, which is added to the litter pool. When the litter pool decomposes, some portion of the carbon within it is recycled to the atmosphere, while the remaining carbon is added to pools of soil organic carbon 1 (fast decomposition rate) or 2 (slow decomposition rate). Finally, decomposed soil organic carbon is recycled to the atmosphere as CO_2.

Water cycles

Figure 3 provides an overview of the water cycle as represented in the model. The ground is composed of three soil layers: soil layer 1, soil layer 2, and soil layer 3. Depth of each soil layer, $Depth_{(1)}$, $Depth_{(2)}$, $Depth_{(3)}$, is 500 mm, 1000 mm, and 1500 mm, respectively. Hydrological and radiation properties of soil is given by 5 grid-specific parameters, *ALBEDO*, *Wsat*, *Wfi*, *Wmat*, and *Wwilt*. Each parameter indicates soil albedo, soil moisture at saturation point, field capacity, matrix potential, and wilting point, respectively. Water can be pooled as snow ($pool_{snow}$) and as water in soil layers 1, 2, and 3 ($pool_{w(1)}$, $pool_{w(2)}$, and $pool_{w(3)}$, respectively). Percolated water from soil layer 3 is immediately removed as runoff.

Daily water flow (in the order of computation)

Precipitation (*prec*) is divided into rainfall ($prec_{rain}$) and snowfall ($prec_{snow}$) using empirical function of the daily mean temperature of air (tmp_{air}) (Ito and Oikawa, 2002):

$$prec_{snow} = prec / [\ 1 + \exp(\ 0.75 \times tmp_{air} - 1.5\ )\ ] \quad (1)$$

$$prec_{rain} = prec - prec_{snow}. \quad (2)$$

Snowfall is added to the snow pool ($pool_{snow}$), which melts as a function of soil temperature (tmp_{soil}):

$$\Delta pool_{snow} = prec_{snow} - tw \quad (3)$$

$$tw = pool_{snow} / [\ 1 + \exp(-0.3\ (\ tmp_{soil} - 10\ )\ )\ ], \quad (4)$$

where *tw* is daily snow melting water. A portion of the rainfall is caught by leaves, and evaporates before reaching the soil surface. The fraction of this intercepted rainfall is a function of leaf area index (*lai* in $m^2 m^{-2}$).

$$ic = \min [prec_{rain}\ , 3.0 \times rain \times (\ 1.0 - \exp(-1.0 \times lai)\ )\ ], \quad (5)$$

where *rain* is expected number of rain in a day, which is calculated using method in Neilson(1992). From the above equations, the daily liquid water to reach the soil surface can be calculated as $prec_{rain} + tw - ic$. Some of this water $pn_{(0)}$ infiltrates soil layer 1, while the rest $(prec_{rain} + tw - ic) - pn_{(0)}$ washes off the surface as runoff (see Appendix A5 for calculation of $pn_{(0)}$).

Daily changes of the soil water storages (in the order of computation)

The daily changes in soil water storage are represented as follows, where ev, $tr_{(n)}$, and $pn_{(n)}$ are the rates of evaporation from soil surface, transpiration from soil layer n, and penetration from soil layer n, respectively':

$$\Delta pool_{w(1)} = (pn_{(0)} - pn_{(1)}) - tr_{(1)} - ev \quad (6)$$

$$\Delta pool_{w(2)} = (pn_{(1)} - pn_{(2)}) - tr_{(2)} \quad (7)$$

$$\Delta pool_{w(3)} = (pn_{(2)} - pn_{(3)}). \quad (8)$$

This model neglects the upward movement of capillary water under dry conditions. The computational methods for penetration and evapotranspiration are detailed in Appendix A5 and A6, respectively.

To control leaf phenology and the rate of photosynthesis as a function of soil water

availability, the physiological status of water availability is defined for each PFT ($stat_{water}$, 0.0–1.0) as follows:

$$stat_{water} = \frac{\max\left(\frac{pool_{w(1)}}{Depth_{(1)}}, \frac{pool_{w(2)}}{Depth_{(2)}}\right) - Wwilt}{Wfi - Wwilt}. \quad (9)$$

When soil temperature is less than 0 °C , $stat_{water}$ is assumed to be zero.

Establishment of Woody PFTs

In the model, new individual trees establish on the last day of each simulation year. It is assumed that establishment only occurs if total precipitation of the current year (in mm) exceeds 20 times the annual mean temperature (in °C) (Köppen, 1936). Each woody PFT has two parameters of climatic range for establishment, following the LPJ–DGVM (Sitch et al., 2003): the maximum coldest-month temperature (TC_{max}), and the minimum growing-degree day ($GDDmin$), as shown in Appendix B5. Both climatic limitations are applied to the running means of the last 20 years. For boreal broad-leaved summergreen trees (BoBS), we assumed that they can only establish when the midday photosynthetically active radiation (PAR, hereafter) that averaged for the previous year exceeded 700 μmol photon m^{-2} s^{-1} at the surface of the grass layer. For tropical and temperate evergreen trees (TrBE, TeNE, TeBE), we additionally assumed that they cannot establish when drought month (monthly means of $stat_{water} < 0.3$) continued more than 6 month in the previous year.

All newly established trees have 0.01 m of $dbh_{sapwood}$, 0.00 m of $dbh_{heartwood}$, and 0 m of

lowest-branch height (i.e., $height = crown_{depth}$). From these properties, tree height ($height$), crown diameter ($crown_{diameter}$), and stem biomass ($mass_{trunk}$) are calculated using allometric and allocation formulas described in the section titled 'tree growth.' These newly established trees initially lack leaves and fine roots, but have 500 g DM of reserve resource ($mass_{stock}$). The biomass of newly established trees is taken from the litter pool of the same forest so that total carbon storage of the forest remains the same.

The floor of the virtual forest is divided into a grid of 1.0 × 1.0–m mesh, and each tree monopolizes one of the mesh boxes. The SEIB–DGVM assumes that crowns of different trees cannot occupy the same space, and thus mesh boxes in which a newly established tree interacts with existing trees are not available for further establishment. For each available mesh box, the same establishment rate, $P_{establish,}$ was assumed.

Establishment of Grass PFTs

For grass PFTs, establishment processes are not treated explicitly. A small amount of grass 'seed' is always assumed to be present, even if the environment is unfavorable to grass survival; densities of grass biomass ($gmass_{leaf}$, $gmass_{root}$, and $gmass_{stock}$) never decrease below their minimum limits (0.1 g m^{-2} for all).

The floor of the virtual forest is disproportionately divided into two sections (90% and 10%), and each section is monopolized by one of the two grass PFTs, namely C_3 and C_4 grass. Thus, the two grass PFTs always coexist in the forest, but one dominates the other, the dominant PFT being distributed throughout the larger fraction. Dominant grass PFT was determined on the last day of each year; the grass PFT that has a higher annual NPP per unit area in the

previous year will be dominant in the following year. When the dominant PFT changes, the biomass properties ($gmass_{leaf}$, $gmass_{root}$, and $gmass_{stock}$) of the two grass PFTs are exchanged so that the total grass biomass of the plot remains the same.

PAR Allocation

For each simulation day, the radiation module of the SEIB–DGVM calculates direct and diffuse components of photosynthetically active radiation at midday (par_{direct} and $par_{diffuse}$, respectively) (see Appendix A2 for the calculation). How these PARs are distributed among trees and grass primarily controls plant growth and competition.

Woody PFTs

Each tree crown is horizontally sliced into 10-cm-deep 'disks,' for which photosynthesis is calculated separately (Fig. 1). The midday PAR that enters disk l of individual n, $par_{wood(l,n)}$, is calculated as follows, where $fpar_{direct(l,n)}$ and $fpar_{diffuse(l)}$ represent the relative intensity of direct and diffuse PAR of disk l of tree n at midday compared to the forest top, respectively:

$$par_{wood(l,n)} = fpar_{direct(l,n)} \times par_{direct} + fpar_{diffuse(l)} \times par_{diffuse}. \quad (10)$$

To obtain $fpar_{direct(l,n)}$, a virtual cylinder with a cross section equal to disk l, was extended from the disk to the direction of the south with angle $0.86 \times sl_{hgt}$, where sl_{hgt} is midday solar angle (Fig. 4). The horizontal line of $0.86 \times sl_{hgt}$ equally divides daily sum of solar radiation into two, when daily changes of solar angle and solar radiation are sin and $\sin^2$, respectively. Then, the total leaf area falling within the cylinder, $fpar_{direct(l,n)}$, was summed using Beer's law

as follows, where $la_{(p)}$ (m^2) is the sum of the leaf area of PFT p within the cylinder, $crown_{area(n)}$ is the cross section of the crown area of tree n, and $EK_{(p)}$ is the vertical light attenuation coefficient of PFT p:

$$fpar_{direct(l,n)} = \exp\left(\frac{-1.0\times\sum_{p=1}^{woody\_pft}(EK_{(p)}\times la_{(p)})}{crown_{area(n)}}\right). \quad (11)$$

Note that we assumed 0.5 for $EK_{(p)}$ for all PFTs. In this calculation, the virtual forest was assumed to repeat; i.e., if the cylinder exited the forest edge at a lower position than the tallest tree, the cylinder would reenter the forest from the opposite edge at the same position in a west–east vertical plane. The calculation of $fpar_{direct(l,n)}$ is the most computationally power-consuming process in the model. Thus, this factor is updated in five-day intervals.

Because diffuse PAR scatters in the sky, we ignored horizontal structures in the forest while calculating its distribution in the forest; all disks at the same height receive the same intensity of diffuse PAR. The relative intensity of diffuse PAR on the disk layer l, $fpar_{diffuse(l)}$, is calculated every day as follows, where $lai_{(l,p)}$ is the leaf area index (m^2 m^{-2}), which is calculated only for PFT p and for leaves above disk layer l:

$$fpar_{diffuse(l)} = \exp\left(-1.0\times\sum_{p=1}^{woody\_pft}(EK_{(p)}\times lai_{(l,p)})\right). \quad (12)$$

Grass PFTs

The midday PAR that reaches the grass layer par_{grass} is calculated every day as follows, where

$lai_{(p)}$ is the leaf area index of woody PFT p in this plot:

$$par_{grass} = \left(par_{direct} + par_{diffuse}\right) \times \exp\left(-1.0 \times \sum_{p=1}^{woody\_pft} \left(eK_{(p)} \times lai_{(p)}\right)\right). \quad (13)$$

This equation assumes that a tree with uniform foliage distributes PAR evenly over the grass layer. As shown in the equation below, $eK_{(p)}$ is the light attenuation coefficient for the direction of the sun at midday. It is calculated every day as a function of solar angle at midday sl_{hgt} (see Appendix A2 for the calculation) and the light attenuation coefficient for vertical direction $EK_{(p)}$:

$$eK_{(p)} = EK_{(p)} / \sin(sl_{hgt}). \quad (14)$$

We should point out that equation 13 should underestimate the par_{grass}, because tree leaves are unevenly distributed in the virtual forest and radiation is exponentially attenuated by the leaves. We chose the present approximation, however, to avoid time-consuming calculation of PAR distribution at the grass layer.

Photosynthesis

To compute photosynthesis values, the SEIB–DGVM assumes that environmental conditions other than PAR intensity (e.g. air temperature, CO_2, and water) are equal among all the leaves, all day. The single-leaf photosynthetic rate is formulated as a simple Michaelis-type function of the intensity of PAR, *par*, where p_{sat} and *lue* are the light-saturated photosynthetic rate and light-use efficiency, respectively (see Appendix A4 for the calculation):

$$p_{single} = \frac{p_{sat} \times lue \times par}{p_{sat} + lue \times par}. \quad (15)$$

Woody PFTs

According to Kuroiwa (1979), a daily change in PAR can be approximated by a sine square function as follows, where *dlen* is day length (hour), and *x* and par_l are intensity of PAR on crown disk *l* at time *t* (hour from sunrise) and at midday, respectively:

$$x = par_l \times \sin^2\left(\pi \times \frac{t}{dlen}\right). \quad (16)$$

By combining equations 16 and 15, and integrating the resultant equation into day length, the daily photosynthetic production on crown disk *l*, $gpp_{(l)}$, is obtained as follows, where constant $12 \cdot 10^{-6} \cdot 3600/0.41505$ is the unit converter from [μmol CO_2 m^{-2} s^{-1}] to [g DM m^{-2} hour m^{-2} s^{-1}] and la_l is the leaf area within crown disk *l*:

$$\begin{aligned} gpp_{(l)} &= 12 \times 10^{-6} \times 3600 \times \frac{1}{0.41505} \times la_{(l)} \times \int_0^{dlen} p_{single}\, \mathrm{d}t \\ &= 0.090936 \times la_{(l)} \times dlen \times p_{sat} \times \left(1 - \frac{1}{\sqrt{1 + lue \times par_{(l)} / p_{sat}}}\right). \end{aligned} \quad (17)$$

Using 17, the daily photosynthetic production is obtained for each crown disk of each individual. These values are summed for each individual tree, and then added to the available resource of the tree, $mass_{available}$.

Grass PFTs

Grass leaves are assumed to be uniformly distributed within the grass layer. Thus, PAR of time t (hour from sunrise) at cumulative grass LAI y ($m^2 m^{-2}$) is calculated as follows, where par_{grass} is PAR at the surface of the grass layer at midday:

$$x = par_{grass} \times \sin^2\left(\pi \frac{t}{dlen}\right) \times e^{-eK \times y}. \quad (18)$$

By combining equations 18 and 15, and integrating the resultant equation into t and y, the daily gross primary production of the grass layer, gpp_g, is calculated as follows (Kuroiwa, 1979), where lai_g is the leaf area index of the grass layer ($m^2 m^{-2}$):

$$\begin{aligned} gpp_g &= 0.090936 \times \int_{y=0}^{lai_g} \int_{t=0}^{dlen} p_{single} \, \mathrm{d}t \, \mathrm{d}y \\ &= 0.090936 \times \frac{2 \times dlen \times p_{sat}}{eK} \times \ln\left(\frac{1 + \sqrt{1 + \frac{par_{grass} \times eK \times lue}{p_{sat}}}}{1 + \sqrt{1 + \frac{par_{grass} \times eK \times lue}{p_{sat}} e^{-eK \times lai_g}}} \right). \end{aligned} \quad (19)$$

The daily photosynthetic production is added to available resource of grass PFTs, $gmass_{available}$.

Canopy Conductance

To compute single-leaf stomatal conductance gs, the SEIB–DGVM adopts a semi empirical model by Ball et al. (1987), modified by Leuning (1995), where $co2_{atm}$ is atmospheric CO_2

concentration, $co2_{cmp}$ is the CO_2 compensation point, and *vpd* is the vapor pressure deficit between saturated and actual vapor pressures:

$$gs = GS_{b1} + \frac{GS_{b2} \times p_{single}}{(co2_{atm} - co2_{cmp})(1 + vpd / GS_{b3})}. \quad (20)$$

Here, GS_{b1}, GS_{b2}, and GS_{b3} are PFT-specific parameters. In the model, *vpd*, $co2_{atm}$, and $co2_{cmp}$ are updated every day, according to Appendix A1 and A4. For each crown disk *l* of each tree *n*, mean daytime stomatal conductance ($gs_{mean(l,n)}$ in mol H_2O m^{-2} s^{-1}) is obtained by combining equations 15, 16, and 20, and integrating the resultant equation into time *t*, averaged over the daytime:

$$gs_{mean(l,n)} = GS_{b1} + \frac{GS_{b2} \times p_{sat}}{(co2_{atm} - co2_{cmp})(1 + vpd / GS_{b3})}\left(1 - \frac{1}{\sqrt{1 + lue \times par_{(l,n)} / p_{sat}}}\right) \quad (21)$$

Thus, mean daytime and whole forest stomatal conductance of woody PFTs, $ccon_{wood}$ (in mol H_2O m^{-2} s^{-1}), is calculated as follows, where *AREA* is the area of the simulation plot (m^2):

$$ccon_{wood} = \sum_n \sum_l \left(gs_{mean(l,n)} \times la_{(l,n)}\right) \Big/ AREA . \quad (22)$$

The mean daytime stomatal conductance for grass PFTs, $ccon_{grass}$ (in mol H_2O m^{-2} s^{-1}), is obtained by combining equations 15, 18, and 20, and integrating the resultant equation into

daytime and cumulative LAI.

$$ccon_{grass} = GS_{b1} \times lai_g + \frac{GS_{b2} \times p_{sat}}{(co2_{atm} - co2_{cmp})(1 + vpd / GS_{b3})} \times \frac{2}{eK} \times \ln\left(\frac{1 + \sqrt{1 + \frac{par_{grass} \times eK \times lue}{p_{sat}}}}{1 + \sqrt{1 + \frac{par_{grass} \times eK \times lue}{p_{sat}} e^{-eK \times lai_g}}} \right) \quad (23)$$

We defined the sum of $ccon_{wood}$ and $ccon_{grass}$ as the mean daytime stomatal conductance of this plot ($ccon$ in mol H_2O m^{-2} s^{-1}).

Growth Respiration

For plants to grow, they require carbohydrates both for their plant-body construction and for biosynthesis. Here, we define construction cost as the required biomass per actual growth (g DM g DM^{-1}). Thus, the amount of growth respiration of organ o is $(RGo - 1.0) \cdot \Delta mass_o$, where RGo is the construction cost of organ o and $\Delta mass_o$ is an biomass increment of organ o. Construction cost can be estimated by combining data on the biochemical composition of organs with knowledge on the biochemical costs of synthesis of all the major compounds, including cellulose, hemicellulose, lignin, protein, lipids, and organic acids (Lambers et al., 1998). Applying this method, Poorter (1994) collected biochemical composition data on various plant species, and then estimated the construction cost of leaves (1.56, mean vale of 123 species), stems (1.44, mean value of 38 species), and roots (1.34, mean value of 35 species). Our model employs these parameters with the following two modifications: for grass PFTs, leaves and stems are grouped together as an 'leaf' and thus the two values are averaged

(i.e., their collective construction cost is 1.50); the above parameters of Poorter (1994) are estimated mainly from grass species, so we employ 1.68 as the construction cost of a woody stem, because lignin synthesis requires a high expenditure of energy. This value is taken from Penning de Vries (1975), but modified by changing the nitrogen source to NO_3 as in Poorter (1994).

Forming and utilizing storage resources ($mass_{stock}$ for woody PFTs and $gmass_{stock}$ for grass PFTs) incur metabolic costs such as the synthesis of a storage organ and remobilization of the nutrients within it (Lambers et al., 1998). We could not find any representative estimates that could be applied to a wide variety of plant species; thus, we assumed that 10% of the biomass is consumed while forming storage structures, and another 10% of the biomass of the storage structure is consumed while utilizing those resources ($RG_{stockin} = 1.1$; $RG_{stockout} = 1.1$).

Maintenance Respiration

In our simulations, maintenance respiration occurs every day irrespective of phenology phase. The carbohydrates required for maintenance respiration is first charged to the available resource and then the remaining requirements are charged to the stock resource. When the sum of these two resources of carbohydrate is not enough to cover the amount charged, 1% of the biomass of all of the living organs is removed. The removed biomass of sapwood changes to heartwood, while the removed biomass of other organs enters the litter pool. Note that maintenance respiration does not occur in heartwood or the stock resource.

For a wide variety of plant organs, the maintenance respiration rate is linearly related to the nitrogen content of living tissue (Ryan, 1991). Incorporating this tendency into our model, we

calculate the daily maintenance respiration of an organ o as follows, where constant RM is the specific respiration rate at 15.0°C (g DM g N^{-1} day^{-1}) and assumed to be 0.10 for all PFT, PN_o is the nitrogen content per biomass of organ o, tmp is air temperature for aboveground organs and soil temperature for underground organs, and qt represents the temperature sensibility:

$$RM \times (mass_o \times PN_o) \times \exp[\frac{\ln(qt)}{10}(tmp - 15.0)]. \quad (24)$$

The temperature sensibility was formulated according to Yokota and Hagihara (1996), as follows:

$$qt = 2.0 \times \exp(-0.009\,(tmp - 15.0)). \quad (25)$$

First, we estimated the nitrogen content of the leaves PN_f for each PFT (Appendix B6) based on a data set from Wright et al. (2004). However, because this data set does not contain a value for boreal needle-leaved deciduous trees (BoND), the value of PN_f for this PFT is taken from an empirical regression equation by Reich et al. (1997), assuming a leaf longevity of three months. Then, assuming that the relative proportions of nitrogen in each organ for any particular PFT are linearly correlated, we calculated PN_s and PN_r as follows, where the coefficients 0.145 and 0.860 are employed by Friend et al. (1997):

$$PNs = 0.145 \times PN_f \quad (26)$$

$$PNr = 0.860 \times PN_f. \quad (27)$$

Turnover

To account for the turnover of organic matter, constant fractions of leaves and fine roots are transformed into litter, while those of sapwood are transformed to heartwood. This turnover occurs every simulation day irrespective of phenology phase. Appendix B6 shows the PFT-specific turnover rates of leaves TO_f; the data set, which is taken from Wright et al. (2004), does not contain a value for boreal needle-leaved deciduous trees (BoND), so the leaf turnover rate of BoND is assumed to be 4 year^{-1} (i.e., a leaf longevity of three months). For deciduous PFTs, leaf turnover rates are corrected as follows, because they drop all leaves at the end of growth phase: max[0.0, TO_f – 365 / (growth days in the last year)]. This correction did not conducted when they act as de facto evergreen (i.e., when switch to the dormant phase have not occurred for 1 yr since last switch to the growth phase). We also employed this corrected turnover rate for calculation of daily maintenance cost of leaves in the equation 35. The turnover rate of sapwood TO_s is assumed to be 0.05 year^{-1} for all PFTs, while the turnover rate of fine roots TO_r is taken from Gill and Jackson (2000).

Phenology

Every deciduous PFT in the model has two phenology phases: a growth phase and a dormant phase. Foliation and growth of deciduous PFTs only occurs during the growth phase. The criteria for switching between the two phases, and the procedure of phase change, are described below.

From Dormant Phase to Growth Phase

Each PFT is classified into the following five phenology types, which differ in submodels. The submodels that initiate the growth phase for summer green woody PFTs (TeBS, BoBS, BoNS) are taken from Botta et al. (2000), based on the global distribution of leaf onset date estimated from remote sensing data. A daily computational time step is applied to each submodel.

・ Summer green broad-leaved woods (TeBS, BoBS)

One of the phenology control variables is $gdd5_{Jan}$, which sums the daily mean air temperature above 5°C starting on 1 January (for the northern hemisphere) and 1 July (for the southern hemisphere). Trees change from the dormant phase to the growth phase when $gdd5_{Jan}$ exceeds $-68 + 638 \times \exp(-0.01 \times i)$, where i is the sum of the days for which the mean air temperature is below 5°C, starting on 1 November (for the northern hemisphere) and 1 May (for the southern hemisphere). Thus, the number of cold days affects the number of days required for phenology change.

・ Summer green needle-leaved woods (BoNS)

The phenology control variable is the number of growing days (*ngd*), defined as the number of days during the preceding 60 days on which the daily mean air temperature is above −5°C. When *ngd* exceeds 15 days, the dormant phase changes into the growth phase.

・ Raingreen woody PFT (TrBR)

When 10 day running average of $stat_{water}$ exceeds 0.5, the dormant phase changes into growth phase.

- Grass PFTs (TeH, TrH)

When optimum leaf area index (lai_{opt}; formulas described in the section titled 'Growth Procedure of Woody PFTs') exceeds 0 for preceding 7 days, the dormant phase changes into the growth phase.

We also assumed that the day of the year (*doy*) of the switch is within the range of 'latitude + 30' to 'latitude + 130' for the northern hemisphere, and '212 − latitude' to '312 − latitude' for the southern hemisphere. However, this constraint is not applied to raingreen woods (TrBR). We also assumed that the switch to the growth phase can only happen 60 days after the last switch to the dormancy phase. For the first 14 days of the growth phase, all of the stock resource is consumed, transformed into available resource at a constant rate. For grass PFTs, this transformation is paused when the optimal leaf area index, lai_{opt}, is reached.

From Growth Phase to Dormant Phase

At day 60 after the leaf onset date, leaf phenology can change to the dormant phase. When this occurs, all of the leaves of woody PFTs and grass PFTs are shed as litter. At this moment, if the stock resource does not satisfy the minimum value (100 g individual^{-1} for woody PFTs, 50 g m^{-2} for grass PFTs), the deficit is supplemented from the litter pool. Each deciduous PFT have distinct criterion to change from the growth phase to the dormant phase. For boreal deciduous woody PFTs (BoBS and BoNS), we used criteria of Arora and Boer (2005),

- Temperate summer green broad-leaved woods (TeBS)

The phenology phase is declared dormant if the 10-day running mean of air temperature falls below 9°C or below the 10-year running mean of the coldest month temperature + 5°C.

- Boreal summer green broad-leaved woods (BoBS)

The phenology phase is declared dormant if soil temperature falls below 2°C.

- Boreal summer green needle-leaved woods (BoNS)

The phenology phase is declared dormant if air temperature falls below –5 °C for successive 7 days.

the 10-day running mean of air temperature falls below 9°C (2°C for BoNS) or below the 10-year running mean of the coldest month temperature + 5°C.

- Raingreen woody PFT (TrBR)

The phenology phase is declared dormant when 10 day running average of $stat_{water}$ falls below 0.5.

- Grass PFTs (TeH, TrH)

The phenology phase is declared dormant if optimum leaf area index (lai_{opt}) falls below 0 for preceding 7 days.

Growth procedure of woody PFTs

The growth process of woody PFTs consists of three procedures with daily, monthly, and

annual time steps. Each procedure employs a dynamic allocation scheme to reduce the parameter requirements.

Daily Computation

During the growth phase, while resource availability ($mass_{available}$) is greater than 0, the following procedures are executed for each individual tree every simulation day.

(1) If the fine root biomass ($mass_{root}$) is less than is required by the functional balance ($mass_{leaf}/FRratio$), the deficit is supplemented from $mass_{available}$. Here, $FRratio$ is the ratio of leaf biomass to fine root biomass satisfying the functional balance. $FRratio$ is assumed to be 1.50 for all woody PFTs and 1.00 for all grass PFTs.

(2) The stock resource ($mass_{stock}$) is supplemented until it becomes equal to the existing leaf mass ($mass_{leaf}$). However, this step is skipped for the first 30 days of the growing season.

(3) The final step of the daily growth procedure is foliation. There are three constraints on the maximum leaf biomass for each individual: crown surface area (max_1), cross-sectional area of sapwood (max_2), and available resource (max_3). These maximum values (in g DM) are defined as follows:

$$max_1 = (crown_{area} + \pi \times crown_{diameter} \times crown_{depth}) \times LAmax/SLA \quad (28)$$

$$max_2 = ALM_1 \times \left[\pi \left(\frac{dbh_{heartwood}}{2} + \frac{dbh_{sapwood}}{2} \right)^2 - \pi \left(\frac{dbh_{heartwood}}{2} \right)^2 \right] / SLA \quad (29)$$

$$max_3 = mass_{available}/RG_f, \quad (30)$$

where the constant *SLA* is the PFT-specific leaf area per unit biomass (Appendix B4). *SLA* is primary taken from data of Wright et al. (2004), but it does not include a value for boreal needle-leaved deciduous trees (BoND); thus, the *SLA* value for this type is derived from an empirical regression equation from Reich et al. (1997), assuming a leaf longevity of three months. *LAmax* is the PFT-specific maximum leaf area per unit crown surface area excluding the bottom soffit. ALM_1 is a constant that represents the required area of transport tissue per unit leaf area (Shinozaki et al. 1964a, b). If the current leaf area is less than the min(max_1, max_2, max_3), the deficit is supplemented from $mass_{available}$.

Monthly Computation

The monthly process of tree growth is outlined below, in the order of execution. For deciduous PFTs, this procedure is omitted during the dormancy phase and for the first three weeks of the growing phase.

(1) Reproduction: If total woody biomass is more than 10 kg, 10% of the available resource ($mass_{available}$) is transformed into litter.

(2) Trunk growth: All of the remaining resource is used for sapwood biomass ($mass_{sapwood}$)

growth. There is no direct allocation to heartwood, which is produced indirectly by slowly converting sapwood. Increments of sapwood biomass are accompanied by growth in sapwood diameter ($dbh_{sapwood}$) and trunk height (*height*). These increments ($\Delta dbh_{sapwood}$ and $\Delta height$) must satisfy the following two trunk mechanics.

(A) Trunk mechanics 1: a relationship between trunk biomass and trunk geometry. Trunk biomass, a function of tree height (*height*) and trunk diameter, is calculated as follows, where ALM_3 is dry mass per unit timber volume (in g DM m^{-3}):

$$mass_{trunk} = ALM_3 \times \pi \left(\frac{dbh_{sapwood} + dbh_{heartwood}}{2}\right)^2 \times height \quad (31)$$

The value of ALM_3 for BoNS was obtained from Schulze et al. (1995), while those of broad-leaved PFTs and evergreen needle-leaved PFTs were calculated by averaging 46 broad-leaved woody species and 24 needle-leaved woody species from Japan; the data were obtained from a table in *The Handbook of Wood Industries* (FFPRI, 1982). It should be noted that the table excluded pioneer woody species, which typically produce low-density timber, and that the SEIB–DGVM assumes that the trunk has a cylindrical shape that extends to the top of the crown (Fig. 1). Thus, the estimated trunk biomass should exceed the actual biomass for the same trunk diameter at bottom with tapered trunk shape; however, because the model includes branches and coarse roots as trunk biomass, this simplification might be justified.

(B) Trunk mechanics 2: a relationship between trunk diameter and maximum tree height for that diameter, calculated as follows, where the parameters *HGTs* and *HGTmax* are the initial growth slope and the maximum tree height for an infinite trunk diameter,

respectively:

$$height \le \left[\frac{1}{HGTs \times (dbh_{sapwood} + dbh_{heartwood})} + \frac{1}{HGTmax} \right]^{-1}. \quad (32)$$

As shown in Appendix B4, *HGTs* and *HGTmax* values for tropical trees and temperate broad-leaved trees are taken from Kohyama et al. (1999); those for temperate needle-leaved trees are from T. Nishimura (unpublished data, 2005); those for BoNS are from Schulze et al. (1995); and for other boreal trees are from Takahashi et al. (2001). In the model, the crowns of different trees cannot occupy the same space. Thus, when the crowns of neighboring trees interfere with tree height, only the trunk diameter expands.

(3) Expansion of a cross-sectional area of the crown:

We used relationships between stem diameter and crown cross-sectional area, based on the inversion of Reineke's rule (Zeide, 2001). Crown expansion is calculated as follows, where the constant ALM_2 is assumed to be 100.0 for every needle-leaved PFT and 200.0 for every broad-leaved PFT:

$$crown_{area} \le ALM_2 \times (dbh_{sapwood} + dbh_{heartwood})^{1.6}. \quad (33)$$

The crown diameter has two constraints: it can neither exceed its maximum limit (CD_{max}) nor expand into neighboring crowns.

Annual Computation

On the last day of each year, the height of the lowest branch increases as a result of purging crown disks, or self pruning of branches, at the bottom of the crown layer. This procedure is conducted even if the tree is in the dormancy phase. A maximum of 10 crown disks can be pruned at one time, each at a depth of 10 cm. Consequently, and because elongation of the lowest branch is linked to crown pruning, the maximum increase in height of the lowest branch is 100 cm year^{-1}. To determine the number of crown disks to purge, we first calculate a variable, $stat_{leaf}$, which represents the expected profit of maintaining a crown disk (g DM day^{-1}), as follows, where gpp_l is the daily photosynthetic production of a crown disk and *cost* is the daily maintenance cost per unit leaf biomass (in g DM g DM day^{-1}):

$$stat_{leaf} = gpp_l - \cos t \times \frac{la}{SLA} \times \frac{1}{10 \times crown_{depth}}. \quad (34)$$

The *cost* variable is calculated daily for each PFT as follows, where *r1* and *r2* are the daily maintenance respiration rates of leaves and fine roots, respectively (g g^{-1} day^{-1}), derived from equation 24 for each PFT:

$$\cos t = \left(r1 + RG_f \times \frac{TO_f}{365} \right) + \left(r2 + RG_r \times \frac{TO_r}{365} \right) \frac{1}{FRratio}. \quad (35)$$

Then, the annual mean of $stat_{leaf}$ for each of the 10 crown groups (1–10 successive disks from the crown bottom) for each tree is calculated. These values are divided by the annual mean of $stat_{leaf}$ of the top crown disk of each tree, and then this value is used to select disks for purging.

Those with values less than ALM_4 are selected for pruning; of these, the group that includes the largest number of crown disks is pruned. It should be noted that pruning is also constrained by $crown_{depth}$, which must always exceed 10 (i.e., >100 cm) and that once a crown disk is pruned, it cannot reestablish (i.e., the height of the lowest branch cannot decrease).

On the last day of each year, the crown center moves horizontally toward the most open direction. This crown movement represents the fact that trees extend their branches into open and bright spaces. Without introducing this plasticity, interference among crowns severely limits the number of tall trees, because crowns of different trees cannot occupy the same space in the SEIB–DGVM. The maximum speed of crown movement is assumed to be 20 cm year^{-1}, and the maximum distance of the movement is equal to half of the crown radius (i.e., the distance between the bole and crown centers is less than half of the crown radius).

Growth Process of Grass PFTs (Daily Computation)

During the growth phase, while resource availability ($gmass_{available}$) is greater than 0, the following procedures are executed every simulation day.

(1) If root biomass ($gmass_{root}$) is less than that required by the functional balance ($gmass_{leaf}/FRratio$), the deficit is supplemented.

(2) The stock resource ($gmass_{stock}$) is supplemented until it becomes equal to the existing leaf biomass ($gmass_{leaf}$). This step is omitted for the first 30 days of the growing season.

(3) The leaf biomass ($gmass_{leaf}$) is supplemented until the leaf area index of the PFT (lai_g)

reaches a weekly running mean equal to the optimal leaf area index lai_{opt}, which maximizes daily net primary production, $gpp_g - cost \times lai_g/SLA$ (derived from equations 19 and 34). This variable is calculated as follows, where *cost* is the cost of maintaining leaves per unit leaf mass per day (see equation 34 for the definition):

$$lai_{opt} = \frac{\ln par_{grass} - \ln\left\{\frac{p_{sat}}{lue}\left[(1 - \frac{cost / SLA}{0.09093 \times dlen \times p_{sat}})^{-2} - 1\right]\right\}}{eK}. \qquad (36)$$

(4) All remaining resource ($gmass_{available}$) is used for reproduction, and then transformed into litter. This step is omitted for the first 30 days of the growing season and when the stock resource is less than 100 g DM m^{-2}.

Mortality (Except Death by Fire)

Mortality is explicitly modeled only for woody PFTs. On the last day of each simulation year, the overall death rate is calculated for each individual tree as a sum of mortality components, which consist of background mortality, heat stress, and bioclimatic limit. These components are derived from the LPJ–DGVM (Sitch et al., 2003). In addition to the above parameters, a tree dies if the NPP of the previous year is less than 10 DM g or if the trunk diameter is more than 1.0 m. It is also assumed that newly established trees do not die in their first year.

Background mortality is related to growth efficiency, which seems to be a sensitive indicator of resistance to environmental stress (Warning, 1983). Although there is no standard formula

for background mortality, the model assumes the following, where *anpp* is the annual sum of net primary production (g DM), la_{mean} is the mean leaf area of the previous year (m^2), and M_1 (≤ 1.0) and M_2 (≥ 1.0) are PFT-specific mortality coefficients:

$$\frac{M_1}{M_2^{\frac{anpp}{la_{mean}}}} . \tag{37}$$

Mortality by heat stress is determined only for boreal woody PFTs (BoNE, BoNS, BoBS). This mortality component, which is based on the sum of daily temperatures, is calculated as follows, where $tmp_{air(d)}$ is the air temperature on day d of the year:

$$\min\left[1.0, \sum_{d=1}^{365} \max\left(0.0, tmp_{air(d)} - 23.0\right) \Big/ 300\right]. \tag{38}$$

Mortality by bioclimatic limit restricts the climate range in which each PFT can survive. If the 20-year mean of the coldest month temperature is less than the PFT-specific limit TC_{min}, all individuals of the PFT die immediately. Boreal needle-leaved summergreen trees (BoNE) have an additional bioclimatic limit: if the 20-year mean of (warmest–coldest monthly air temperature) is less than 43°C, all trees of the PFT die. Biomass of dead trees is forming new litter.

Disturbance by Fire

Fire is the only disturbance currently incorporated in the SEIB–DGVM. We employed the global fire model of Thonicke et al. (2001), which was developed for the LPJ–DGVM. On the

last day of each simulation year, if the fuel load (litter + aboveground biomass) satisfies the minimum threshold (200 g C m^{-2}), the probability of fire is calculated as a function of the moisture content of soil layer 1 as follows:

$$s \times \exp\left(\frac{s-1}{0.45(s-1)^3 + 2.83(s-1)^2 + 2.96(s-1) + 1.04}\right), \tag{39}$$

, where variable s is

$$s = \sum_{day=1}^{365} \exp\left[-\pi\left(\frac{pool_{w(1)}}{W_{sat} \times Depth_{(1)}} \times \frac{1}{m_e}\right)^2\right] \Big/ 365. \tag{40}$$

Variable m_e in equation 40, which takes into consideration the difference in fire extinction efficiency between woody and grass PFTs, is defined as 0.3 × (aboveground biomass of trees/total aboveground biomass) + 0.2 × (leaf biomass of grass/total aboveground biomass). The model also assumes that fire cannot occur in two consecutive years.

The fraction of individuals killed in a fire depends on PFT fire resistance (M_3, Appendix B5). During a fire, all leaf biomass of grass, all leaf biomass of dead and surviving trees, half of the trunk biomass of dead trees, and half of the litter pool are released into the atmosphere as CO_2, while the remaining biomass of dead trees is transformed into litter. In response to fire, the phenology phase of all deciduous PFTs changes to dormant (they reenter the growth phase as described previously in the section titled 'Phenology'). If the stock resource of grass PFTs ($gmass_{stock}$) does not satisfy the minimum value (50 g DM m^{-2}) after fire, the deficit is

supplemented from litter.

Soil Respiration

The decomposition of litter and soil organic carbon is calculated for each month. The SEIB–DGVM employs the soil respiration module of the DEMETER-1 (Foley, 1995) with some simplifications. The average annual decomposition rate of litter pool k_l is calculated as follows, where *aet* is the actual evapotranspiration in the previous year:

$$k_l = \min\left(1.0, \frac{10^{(-1.4553+0.0014175\times aet)}}{12}\right). \quad (41)$$

Seventy percent of the decomposed litter carbon is released into the atmosphere as CO_2, and the remaining 30% becomes soil organic carbon. The partitioning coefficients for soil organic carbon flowing into the fast and slow decomposition pools are 0.985 and 0.015, respectively.

According to Foley (1995), the mean turnover rates for the fast and slow soil organic carbon (TO_{fast}, TO_{slow}) at 20°C and ample soil moisture are 1/15 year^{-1} and 1/750 year^{-1}, respectively. Actual monthly turnover rates (k_n month^{-1}), which are adjusted according to soil environment, are calculated as follows, where g and f are functions of the monthly mean air temperature and soil moisture, respectively:

$$k_n = \left[\frac{TO_n}{12}\times \mathrm{g}(tmp_{soil})\times \mathrm{f}(pool_{w(1)})\right] \quad (42)$$

These functions are defined as follows:

$$g(tmp_{soil}) = \exp\left(308.56 \times \left(\frac{1}{66.02} - \frac{1}{tmp_{soil} + 46.02}\right)\right) \quad (43)$$

$$f(pool_{w(1)}) = 0.25 + 0.75\left(\frac{pool_{w(1)}}{W_{sat} \times Depth_{(1)}}\right) \quad (44)$$

In Foley (1995), the temperature effect g (tmp_{soil}) is an exponential function. However, this underestimates the soil turnover rate for cold regions, and thus we employ the function of Lloyd and Taylor (1994). All decomposed soil organic carbon is released into the atmosphere as CO_2.

Input Data

Climatic data (air temperature, soil temperature, precipitation, total cloud cover, specific humidity, and wind velocity) are taken from the NCEP (National Center for Environmental Prediction) Reanalysis Project at the NOAA–CIRES (National Oceanic and Atmospheric Administration/Cooperative Institute for Research in Environmental Sciences) Climate Diagnostics Center (www.cdc.noaa.gov), Boulder, Colorado, USA (Kistler et al., 2001). These data were averaged over 1990–1999 for each day of the year and input repeatedly for each simulation year. For soil properties, we used input data from GSWP2 (Global Soil Wetness Project 2, www.iges.org/gswp). Resolutions of the climatic and soil data are T62 Gaussian grid (192 x 94 points) and 1-degree grids (360 x 180 points), respectively. The concentration of CO_2 in the air is assumed to be 355 ppm for all locations and all days of every year.

Parameter Tuning

Grass PFTs

The aboveground primary production in grasslands, at a regional scale, is mainly regulated by annual precipitation. From observations of 100 ecological regions encompassing 9498 sites along the Central Grassland Region of the United States, Sala (2001) formulated the regression equation between aboveground net primary production (*ANPP* in g DM m^{-2} $year^{-1}$) and mean annual precipitation (*APPT* in mm $year^{-1}$) as $ANPP = -34 + 0.60\ APPT$. Based on 13 sites in Asia, Sala (2001) formulated a very similar regression equation, $ANPP = -30 + 0.59\ APPT$. By adjusting the parameter *PMAX* of grass PFTs (TrH and TeH) and a coefficient in the equation A49 and A50, we tried to reconstruct this trend in Central Plains Experimental Range (Colorado: 40.82ºN, 104.77ºW; annual average air temperature 6.2ºC). The precipitation data were multiplied by consecutive constants to come up with a climatic data set with different annual precipitation levels. With these climatic data, 100-year simulations from bare ground were conducted for each site, assuming that trees could not establish; the *ANPP* of the 100-year time period was employed as the target variable. Calibration results are shown in Figure 5. The simulation adequately represented the observed correlation.

Woody PFTs

We adjusted the model to reconstruct field observations in terms of tree frequency (density, which reflects forest size structure and total woody biomass) for each size class, and the relationship between tree size and growth rate (which reflects competition among trees of different sizes and the incremental rate of total woody biomass in the forest). Thus, this procedure enabled us to capture the most essential dynamic and production properties in the

forest. The index of tree size is trunk diameter at breast height (DBH).

This adjustment is conducted for each woody PFT by employing *PMAX*, ALM_1, ALM_4, *LAmax*, $P_{establish}$, M_1, and M_2 as tuning parameters. For each adjustment, we collected field data on which dominant trees could be exclusively categorized into the target PFT (Table 2). Our climatic data are on a coarse geographic scale; thus, when station data were available, the annual mean air temperature and annual precipitation were adjusted to the actual values of each observation site. Altitude is also adjusted to the observation site. For each simulation adjustment, we assumed that the target woody PFT only establishes. Results of these adjustments are shown in Figure 6. The PFTs TrBR, TeNE, and BoNS are substituted for those of TrBE, TeBE, and BoNE, because we could not find dynamic data for forests in which the latter PFTs exclusively dominate.

Simulations

Zone-specific patterns of Succession

We compared the post-disturbance succession among tropical, temperate, and boreal regions. Each region was represented by Shiretoko, Ogawa, and Serimbu, respectively. In this simulation, forest fire was induced for disturbance. Although fire rarely occurs in some of these regions, it can be thought of as an analog of other disturbances such as logging and shifting agriculture. After a 1000-year spin-up, a 200-year simulation following a fire was repeated 10 times successively; thus, in all, a 3000-year simulation was performed for each site. Ten repeats of each site were averaged to extract general trends of post-fire succession. In

these simulations, fire was not allowed to occur until the start of a new repeat. Only one woody PFT was allowed to establish at each site: BoNE in the boreal region, TeBS in the temperate region, and TrBE in the tropical region.

Figure 7 compares the changes in the annual maximum LAI among the simulation sites. For all of the sites, grass leaves quickly appeared after disturbance, and woody leaves gradually replaced them. This change was delayed for the boreal site, corresponding to its slow growth rate of trees. These results indicate that frequent disturbance increases the proportion of grassland in a region, and this effect continues longer for boreal regions. In the temperate and boreal sites, a considerable amount of grass LAI remained after the formation of the climax forest. This is because the floor of deciduous forests remains bright in early spring in temperate regions, while tree density is relatively low in boreal forests.

Figures 8 and 9 compare the changes in the carbon pool and fluxes among simulation sites. Similar to the patterns of LAI change, biomass accumulates faster in warmer sites. At equilibrium, the proportion of the total available carbon in biomass is Tropical > Temperate > Boreal, while the proportion in litter and soil is Boreal > Temperate > Tropical. The large carbon stock in the boreal site is due to the low soil respiration rate under cold climate. These simulated carbon dynamics along the succession are within accepted ranges of observations for each climatic zone (Pregitzer and Euskirchen, 2004). In addition, comparing the succession of LAI to that of biomass indicates that saturation of LAI precedes that of biomass. This finding corresponds to general observations of natural succession (Kira and Shidei, 1967).

Figure 10 shows the seasonal changes in water flux 200-years after simulated fire. In addition to the three sites used in previous simulations, we included the simulation results of the Central Plain site, in which no trees were allowed to establish, to add a grassland ecosystem for comparison. The amount of interception and transpiration was always present at the tropical site, while it fluctuated according to season at the other sites. This difference in transpiration and interception activity corresponds with seasonal changes in the LAI of each site (i.e., only the tropical site was covered by a evergreen PFT). All sites except grassland, a substantial amount of water was lost through runoff.

Effects of Spatially-Explicit and Individual-Based structure on Succession

The most unique property of the SEIB–DGVM is the spatially-explicit individual-based representation, which enables the model to simulate time lags between climate change and vegetation change without adding other parameters. To demonstrate this potential, we conducted experiments to examine the effects of initial conditions on the patterns of succession after climate change. We selected Yakushima as the study site (Table 2; mean annual air temperature 16.4˚C, annual precipitation 3200 mm), where a parameter tuning of TeBE was conducted. We compared the results between two experiments for which the climatic data were identical, but spin-ups varied. For the spin-up in experiment 1, 10˚C was subtracted from the daily air and soil temperatures of the original climate data. In experiment 2, the daily precipitation of the original climate data was divided by 10. After a 500-year spin-up, a 500-year simulation was conducted. The available mesh-points for tree establishment were equally split by each woody PFT that could establish under the given climatic conditions. Each experiment was repeated for 10 times, and these results were averaged to extract general trends.

Figure 11 compares the changes in physiognomy of the experiments (one typical result of 10 times repeats). Following the spin-up, TeNE dominated in experiment 1, while C_3 grass dominated in experiment 2. Although in both experiments, TeBE and TeBS dominated almost exclusively after completing the 500-years simulation; large trees of TeNE remained for more than 100 years in experiment 1, and they had suppressed the invasion and growth of TeBE and TeBS though occupying establishment sites, occupying available space in crown layer, and one-sided competition for sunlight. This difference in the time course between the experiments is clearly represented by changes in biomass (Fig. 12). For example, the time for the sum of TeBE and TeBS to reach 100 Mg C ha^{-1} was around 135 years in experiment 1, but only 55 years in experiment 2. In experiment 1, TeNE biomass remained high for more than 200 years after climate change, indicating that large trees, which experience favorable sunlight conditions, persisted for a long time even when climate change altered the potential favored species. This time lag between climate change and vegetation change should be much greater if seed dispersal distance is assumed to be about 1 km (Kohyama and Shigesada, 1995; Kohyama, 2005; Takenaka, 2005). Thus, the time lag in this simulation represents a minimum estimate of natural conditions, in which the available seeds are strongly biased toward the present vegetation.

We also examined how these succession pattern is affected by horizontal distribution of sunlight. We conducted experiment 3 and 4 under assumption of horizontally homogeneous for PAR distribution; distribution of direct PAR among tree crowns was calculated using same method of diffused PAR. Excepting the PAR allocation, experiment 3 and 4 share identical protocols of experiment 1 and 2, respectively. When succession started from forest ecosystem, this assumption delayed replacement of dominant PFT; in rank order of biomass, sum of TeBS

and TeBE exceeds TeNE after around 105 years for experiment 1, while 155 years for experiment 3 (Fig. 12). On the other hand, when starting from grassland, no conspicuous effects of PAR distribution were not observed (experiment 2 and 4 in Figs. 11 and 12).

Biome Distribution on Global Scale

We conducted a global-scale simulation with a T42 (128 × 64 points) grid mesh. Each of the points was represented by a 30 × 30-m virtual forest, and a 500-year simulation, beginning with bare ground, was conducted. Figure 13 compares the simulated vegetation map with a natural vegetation map. The classification scheme of vegetation types and the natural vegetation map were taken from Haxeltine and Prentice (1996) with some modifications to reduce the number of vegetation types (Appendix B9). Note that the natural vegetation map is derived from vegetation data only and is not in any way derived from climate data or the output of any model.

SEIB–DGVM reasonably reconstructed distributions of boreal forest and tropical-rain-forest. Distribution of temperate-deciduous-forest was also in good agreement except for Atlantic side of Europe. On the other hand, temperate-evergreen-forest was sparsely appeared, although it dominates in southeast China for the natural vegetation. The most prominent disagreement was found for drought-adapted vegetations. For example, in Africa and Australia, grassland / savanna / steppe distributes wetter regions for simulation than for natural vegetation. Likewise, tropical-deciduous-forest and xeric woodland / scrub were rarely appeared for the simulation.

Discussion

Local-scale evaluations have shown that the model can reproduce climate zone-specific patterns of succession from grasslands to forests. Furthermore, simulated carbon dynamics during succession are within accepted ranges of observations for each climatic zone, and simulated annual changes in water flux correspond with seasonal changes in the LAI. Theses results are the preliminary steps toward global applications, and actually, global scale simulation did not always reconstructed potential vegetation distribution. However, our results imply that the SEIB–DGVM has ability to portray the basic behaviors of terrestrial ecosystems in a wide variety of climatic zones.

The SEIB–DGVM also simulated 'inertia' of physiognomy to climate change without any additional parameterizations. The grassland ecosystem has shorter time lag of vegetation change than forest ecosystem, where growth rate of newly established trees are primary controlled by existing trees through its absorption of sunlight and occupation of available space. It was also demonstrated that the time lag of vegetation change elongated under the assumption of horizontal homogeneity of sunlight distribution. The underlying cause of this delay was probably as follows; due to the assumption of horizontal homogeneity, small trees under a gap cannot grow rapidly to occupy the canopy layer, inhibiting quick increment of the total amount of PAR received by the newly dominating PFT. This result indicates the potential importance of horizontal heterogeneity for predicting transitional behavior of vegetation under changing climate.

To distribute sunlight among trees, most gap models employ a much simpler approach than

SEIB–DGVM (Reviewed by Bugmann, 2001). One of the most mechanistical approach was used by SORTIE (Pacala and Deutschman, 1995). In SORTIE, light-availability-index is calculated for each tree, based on information of the spatial relationships among crowns and information of the sun movement throughout the growing season. By substituting this index to empirical relationships observed in a forest, growth rate was calculated for each individual. On the other hand, SEIB–DGVM uses thin crown disk as the 'unit' of sunlight allocation. This representation enables to treat prominent effect of self shading in low latitude area as well as prominent effect of incoming radiation from side of the crown in high latitude area, without adding empirical parameterizations. For global application, the methodology of SEIB–DGVM might be more advantageous to that of SORTIE, which requires empirical parameterization for each forest to apply the model.

Among existing DGVMs, the SEIB–DGVM is one of the most mechanistically based models in terms of population/community scale of individual interference. Yet it contains some oversimplifications. First, all terrestrial plants are represented by only 10 PFTs, primary due to conserve effort for parameter estimation. These PFTs do not contain shrub species, which dominates for arid and semiarid regions, and this may be the most conspicuous reason for inferiority of drought-adapted vegetations in global scale simulation. Second, the establishment rate of woody PFTs was assumed to be independent of environmental factors. In natural vegetations, environmental conditions play a major role in plant dynamics; establishment is a complex and diverse process that is regulated by seed dormancy, shade tolerance of seedlings and saplings, vegetative propagation ability of mature trees, and other factors (Greene et al., 1999). This complexity and diversification of the establishment process make it difficult to treat the process mechanistically in global-scale models. One possible

solution would be to formulate an establishment rate as an empirical rule for each vegetation type. For example, in the vegetation-dynamics model ALFRESCO (Starfield and Chapin, 1996), patterns of establishment are implicitly included in the rules of transition among vegetation types, and this model successfully simulated the dynamic behavior of vegetation mosaic in Alaskan tundra-boreal forest. Finally, the SEIB–DGVM ignores geological heterogeneity within the grid box; each grid box (ca. 200 × 200 km) is represented by a small virtual forest of 30 × 30 m. Previous DGVMs with highly simplified structures have implicitly included heterogeneity as a parameter. However, as models begin to more accurately reflect reality, the relative importance of this matter increases. Thus, to increase simulation accuracy, we must find a novel way of scaling up in the future.

To this end, we are anxious to include more details in the model. There is a trend in terrestrial ecosystem models toward increasing the mechanisms and feedback loops (Pitman, 2003). However, great caution should be taken when adding new processes to models, because complicated models are capable of amplifying errors in multiple directions, which obscure the relationships between cause and effect. Nonetheless, as there is not enough data to treat the responses of terrestrial ecosystem to climate change in a highly parameterized model, essential processes should be included at least in simple formulations. Terrestrial ecosystems are complex with diverse processes, and thus this task is not feasible without collaborating with field ecologists. The SEIB–DGVM can play a central role in such collaborations. Because this model is formulated to the scale at which field biologists work, the measurements of relevant parameters and data comparisons are relatively straightforward.

Appendix A

A1. Atmospheric environments (computed daily)

Atmospheric conditions were calculated daily based on input climate data. Air pressure (*ap* in hPa) was approximated by site altitude (*ALT* in m) and air temperature (tmp_{air} in °C):

$$ap = 1013.25 \times \exp\left(\frac{-0.2838472 \times ALT}{8.3144(tmp_{air} + 273.15)}\right), \quad \text{(A1)}$$

where the multiplier 1013.25 is the control air pressure (in hPa) at sea level at 15°C, and the multiplier 8.3144 is the universal gas constant (in J mol^{-1} K^{-1}). Actual vapor pressure (*vp* in hPa) was a function of air pressure *ap* and humidity *humid* (g g^{-1}):

$$vp = \frac{ap \times humid}{0.622 + 0.378 \times humid}, \quad \text{(A2)}$$

The saturated vapor pressure vp_{sat} (hPa) was given by Tetens' equation:

$$vp_{sat} = 6.1078 \times 10^{\frac{7.5 tmp_{air}}{237.3 + tmp_{air}}} \quad (tmp_{air} > 0.0) \quad \text{(A3)}$$

$$vp_{sat} = 6.1078 \times 10^{\frac{9.5 tmp_{air}}{265.3 + tmp_{air}}} \quad (tmp_{air} \le 0.0). \quad \text{(A4)}$$

The vapor pressure deficit *vpd* (hPa) is the difference between saturated and actual vapor pressures:

$$vpd = vp_{sat} - vp. \tag{A5}$$

The slope of saturated vapor pressure $slope_{vps}$ (hPa °C^{-1}) is:

$$slope_{vps} = \frac{6.1078 \times (2500 - 2.4tmp_{air})}{0.4615(tmp_{air} + 273.15)^2} \times 10^{\frac{7.5tmp_{air}}{237.3+tmp_{air}}} \quad (tmp_{air} > 0.0) \tag{A6}$$

$$slope_{vps} = \frac{6.1078 \times 2834.0}{0.4615(tmp_{air} + 273.15)^2} \times 10^{\frac{9.5tmp_{air}}{265.3+tmp_{air}}} \quad (tmp_{air} \le 0.0). \tag{A7}$$

The density of air *dnsa* (kg m^{-3}) is:

$$dnsa = 1.293 \frac{ZAT}{tmp_{air} + ZAT} \times \frac{ap}{1013.25} \times \left(1 - 0.378 \frac{vp}{ap}\right). \tag{A8}$$

A2. Solar radiation (computed daily)

Angular solar elevation above the horizontal at midday (sl_{hgt}) was calculated by the following equations:

$$\sin(sl_{hgt}) = \sin(LAT) \times \sin(sl_{dec}) + \cos(LAT) \times \cos(sl_{dec}), \quad \text{(A9)}$$

where LAT is the site latitude ($-90 \leq LAT \leq 90$ in degree) and sl_{dec} is the solar declination of the earth's orbit in degrees. sl_{dec} has a maximum value of 23.4 on the summer solstice, and a minimum value of −23.4 on the winter solstice, and a value of 0 on equinox days; thus, it can be approximated by the following equation:

$$sl_{dec} = 23.4 \sin(360 \times (doy - 81)/365), \quad \text{(A10)}$$

where doy is the days of the year (1–365, ignoring leap years). Using sl_{dec}, the hourly angle of the sun from sunrise to midday can be calculated as $\arccos(-\tan(LAT) \times \tan(sl_{dec}))$; thus, the day length in hours ($dlen$) will be:

$$dlen = 2 [\arccos(-\tan(LAT) \times \tan(sl_{dec}))/15]. \quad \text{(A11)}$$

Shortwave radiation at the top of the atmosphere at midday (rad_{intact} in W m^{-2}) is a function of sl_{hgt}:

$$rad_{intact} = 1367 \times \sin(sl_{hgt}) \times (ESD_{mean}/ESD)^2, \quad \text{(A12)}$$

where the multiplier 1367 is a solar constant (in W m^{-2}), ESD is the distance between the sun and the earth (in km), and ESD_{mean} represents the annual mean ESD ($=1.46 \cdot 10^8$ km).

$(ESD_{mean}/ESD)^2$ can be approximated by:

$$(ESD_{mean}/ESD)^2 = 1.000111 + 0.034221 \cos(x) + 0.00128 \sin(x) + 0.000719 \cos(2x) + 0.000077 \sin(2x), \quad \text{(A13)}$$

where x is the seasonal angle of the earth's orbit ($x = 360 \times doy/365$). In the troposphere, the incident solar radiation rad_{intact} (W m^{-2}) is attenuated by clouds and airborne particles. This effect has been empirically formulated as a function of cloud cover ($0.0 \leq cloud \leq 0.8$) by Iqbal (1983), as follows:

$$rad = rad_{intact} \times (0.8964 - 0.5392\ cloud), \quad \text{(A14)}$$

where rad is the amount of solar radiation that reaches to the biosphere (in W m^{-2}).

In addition to this attenuation effect on irradiance, scattering in the atmosphere optically alters the ratio between direct and diffuse radiation:

$$rad_{diffuse} = rad \times [0.958 - 0.982\ (rad/rad_{intact})] \quad \text{(A15)}$$

$$rad_{direct} = rad - rad_{diffuse}, \quad \text{(A16)}$$

where $rad_{diffuse}$ and rad_{direct} are diffuse radiation and direct radiation within *rad*, respectively. Diffuse and direct radiation differ in their fractional content of photosynthetically active radiation (PAR: 400–700 nm) in the total spectrum; diffuse radiation contains 57%, while direct radiation contains 43%. Thus, photosynthetic photon flux density of PAR is given by the following:

$$par_{diffuse} = 4.2 \times 0.57 \times rad_{diffuse} \quad \text{(A17)}$$

$$par_{direct} = 4.6 \times 0.43 \times rad_{direct} \quad \text{(A18)}$$

$$par = par_{diffuse} + par_{direct} \quad \text{(A19)}$$

where *par* is photosynthetically active radiation at midday (in μmol photon m^{-2} s^{-1}), and $par_{diffuse}$ and par_{direct} are the diffused and direct radiation components of *par*. The multipliers 4.2 and 4.6 are for unit conversion from [W m^{-2}] to [μmol photons m^{-2} s^{-1}] for diffuse and direct radiation, respectively (Larcher, 1995).

A3. Net Radiation (Computed Daily)

To estimate the transpiration rate of leaves and the evaporation rate of soil, the net radiation at vegetation ($radnet_{veg}$ in W m^{-2}) and at the soil surface ($radnet_{soil}$ in W m^{-2}) were calculated as:

$$radnet_{veg} = [rad \times (1 - albedo_{veg}) + radnet_{long}] \times (1 - ir) \quad \text{(A20)}$$

$$radnet_{soil} = [rad \times (1 - albedo_{soil}) + radnet_{long}] \times ir, \quad \text{(A21)}$$

where ir is the shortwave interception by leaves:

$$ir = \exp\left(\sum_{p}^{pft}\left(-eK_p \times lai_p\right)\right) \quad \text{(A22)}$$

and $albedo_{veg}$ and $albedo_{soil}$ are the albedo of vegetation and the soil surface, respectively; $albedo_{veg}$ was assumed to be 0.24 for forest biome and 0.15 for other biome (Jones 1992). On the other hand, $albedo_{soil}$ was assumed be a function of soil albedo ($ALBEDO$) and the amount of snow on the ground:

$$albedo_{soil} = ALBEDO + (0.7 - ALBEDO)/[1 + \exp(-0.05(pool_{snow} - 70.0))]. \quad \text{(A23)}$$

The $radnet_{long}$ is net long-wave radiation, which is estimated by the following empirical formula:

$$radnet_{long} = 5.67 \times 10^{-8} \times (tmp_{air} + 273.15)^4 \times (1 - 0.65\ cloud) \times [0.39 + 0.058/(vp + 1.0)], \quad \text{(A24)}$$

where the constant 5.67×10^{-8} is Stefan–Boltzmann's constant (in W m^{-2} K^{-4}).

A4. Parameters of Photosynthesis and Stomatal Conductance (Computed Daily)

Appendix B7 shows the definition of PFT-specific photosynthesis parameters. To estimate photosynthesis and stomatal conductance, midday photosynthetic rates at the top of the leaf layer (p_{top} in μmol CO_2 m^{-2} s^{-1}) were calculated for each PFT every simulation day, using equation (15):

$$p_{top} = \frac{p_{sat} \times lue \times x}{p_{sat} + lue \times x}, \quad \text{(A25)}$$

where p_{sat} is single-leaf photosynthetic rate under light saturation (in μmol CO_2 m^{-2} s^{-1}). x is the PAR at the top of the leaf layer (in μmol photon m^{-2} s^{-1}). In woody PFTs, we substituted the PAR above tree canopies for x; in grass PFTs, we substituted the PAR below tree canopies for x. *lue* is the light-use efficiency of photosynthesis (in mol CO_2 mol $photon^{-1}$), which is formulated to conform to the data in Osmond et al. (1980) as follows:

$$lue = LUE \times \frac{52 - tmp_{air}}{3.5 + 0.75(52 - tmp_{air})} \times \frac{co2_{cell}}{90 + 0.6 \times co2_{cell}} \quad \text{(for } C_3 \text{ PFTs)} \quad \text{(A26)}$$

$$lue = LUE \quad \text{(for } C_4 \text{ PFTs)}, \quad \text{(A27)}$$

where LUE is the potential maximum value, and $co2_{cell}$ is the intercellular CO_2 concentration (in μmol mol^{-1}). The single-leaf photosynthetic rate, $p_{sat,}$ under light saturation (in μmol CO_2

m^{-2} s^{-1}), is calculated by multiplying its potential maximum of photosynthetic rate (*PMAX*) by the coefficients of temperature, CO_2 level, and soil water effects (ce_{tmp}, ce_{co2}, and ce_{water}, respectively):

$$p_{sat} = PMAX \times ce_{tmp} \times ce_{co2} \times ce_{water}. \quad \text{(A28)}$$

ce_{tmp}, the temperature-dependent function of p_{sat}, is a bell-shaped curve that reaches the maximum (1.0) at the optimum temperature and tapers off in warmer or cooler temperatures (Raich et al., 1991):

$$ce_{tmp} = \frac{(tmp_{air} - T_{\max})(tmp_{air} - T_{\min})}{(tmp_{air} - T_{\max})(tmp_{air} - T_{\min}) - (tmp_{air} - t_{\text{opt}})^2}, \quad \text{(A29)}$$

where T_{max}, T_{min}, and t_{opt} are the PFT-specific maximum, minimum, and optimum temperature for photosynthesis, respectively (in °C). t_{opt} increases with the intercellular CO_2 concentration because of photorespiration:

$$t_{opt} = T_{opt0} + 0.01\ co2_{cell} \quad \text{(A30)}$$

where T_{opt0} is the minimum value of t_{opt} at a very low $co2_{cell}$. For grass PFTs, t_{opt} is assumed to be a 20-year running mean of air temperature in the growth phase (maximum range 10°C–30°C for TeH and 20°C–40°C for TrH), because grass PFTs includes a varieties of species adapted to a wide range of climatic zones.

The ce_{co2}, the CO_2-dependent function of p_{sat}, is expressed by a Michaelis-type function:

$$ce_{co2} = 0.30 + 0.70 \times \frac{co2_{cell} - co2_{cmp}}{KM + co2_{cell}} \quad \text{(for } C_3 \text{ PFTs)} \quad \text{(A31)}$$

$$ce_{co2} = 0.50 + 0.50 \times \frac{co2_{cell} - co2_{cmp}}{KM + co2_{cell}} \quad \text{(for } C_4 \text{ PFTs),} \quad \text{(A32)}$$

where KM is the coefficient of CO_2 concentration sensitivity; $co2_{cmp}$ is the CO_2 compensation point, which is adjusted by temperature for C_3 species (Brooks and Farquhar, 1985).

$$co2_{cmp} = CO2cmp\left[1 + 0.0451(tmp_{air} - 20) + 0.000347(tmp_{air} - 20)^2\right] \quad \text{(for } C_3 \text{ PFTs)} \quad \text{(A33)}$$

$$co2_{cmp} = CO2cmp \quad \text{(for } C_4 \text{ PFTs), (A35)}$$

where $CO2cmp$ is the control value of $co2_{cmp}$ at 20°C; ce_{water}, the water availability effect coefficient of p_{sat}, is calculated as follows:

$$ce_{water} = \sqrt{stat_{water}}\,. \quad \text{(A35)}$$

The midday leaf stomatal conductance of H_2O at the top of the leaf layer gs_{top} (mol H_2O m^{-2} s^{-1}), is obtained by equation 20:

$$gs_{top} = GS_{b1} + \frac{GS_{b2} \times p_{top}}{(co2_{atm} - co2_{cmp})(1 + vpd / GS_{b3})}, \quad \text{(A36)}$$

where GS_{b1}, GS_{b2}, and GS_{b3} are PFT-specific parameters; gs_{top} affects the intercellular CO_2 concentration ($co2_{cell}$ in μmol mol^{-1}) following Leuning (1990):

$$co2_{cell} = co2_{atm} - \frac{p_{top}}{gs_{top} / 1.56}, \quad \text{(A37)}$$

where 1.56 is a factor to convert gs into CO_2 conductance. Using equations A25 through A37, we calculated p_{top}, lue, and gs_{top} of each PFT every simulation day.

A5. Soil water percolation (daily computation)

Water infiltration, percolation and runoff were simulated daily with a modified version of a submodel of MAPPS (Neilson, 1995), which is based on Darcy's law (Hillel, 1982). Calculations were made in the following order: (1) infiltration, (2) percolation from soil layer 1 to 2, (3) percolation from soil layer 2 to 3.

Daily infiltrated water to soil layer 1, $pn_{(0)}$, is:

$$pn_{(0)} = prec_{rain} - ic + tw, \quad \frac{pool_{w(1)}}{Depth_{(1)}} \le W_{mat} \quad \text{(A38)}$$

$$pn_{(0)} = (prec_{rain} - ic + tw)\left\{1 - \left[\frac{(pool_{w(1)}/Depth_{(1)}) - W_{mat}}{W_{sat} - W_{mat}}\right]^{1.4}\right\}, \quad W_{mat} < \frac{pool_{w(1)}}{Depth_{(1)}} \le W_{fi} \quad \text{(A39)}$$

$$pn_{(0)} = 0.0\,, \quad W_{fi} < \frac{pool_{w(1)}}{Depth_{(1)}}, \quad \text{(A40)}$$

where W_{mat}, W_{sat} and W_{fi} are the soil moisture at matrix potential, saturation point, and field capacity, respectively. These are location-specific parameters. $Depth_{(n)}$ is the depth of soil layer n, which is assumed to be constant irrespective of location ($Depth_{(1)}$ = 500 mm, $Depth_{(2)}$ = 1000 mm, and $Depth_{(3)}$= 1500 mm). The constant 1.4 is an infiltration parameter, which is adjusted daily (unpublished data of Conklin and Neilson, 2005). All daily excess water at the soil surface is removed as runoff water.

Water in soil layer n is percolated to the next layer according to the following:

$$pn_{(n)} = K_{s1(n)}\left(pool_{w(n)} - W_{fi} \times Depth_{(n)}\right)\left(\frac{pool_{w(n)}/Depth_{(n)} - W_{fi}}{W_{sat} - W_{fi}}\right)^{K_{s2(n)}}, \quad W_{fi} < \frac{pool_{w(n)}}{Depth_{(n)}}$$

(A41)

$$pn_{(n)} = K_{u1(n)}\left(pool_{w(n)} - W_{mat} \times Depth_{(n)}\right)\left(\frac{pool_{w(n)}/Depth_{(n)} - W_{mat}}{W_{sat} - W_{mat}}\right)^{K_{u2(n)}}, \quad W_{mat} < \frac{pool_{w(n)}}{Depth_{(n)}} \le W_{fi}$$

(A42)

$$pn_{(n)} = 0.0, \quad \frac{pool_{w(n)}}{Depth_{(n)}} \le W_{mat} \,. \tag{A43}$$

The coefficients $K_{u1(n)}$, $K_{u2(n)}$, $K_{s1(n)}$, and $K_{s2(n)}$ are adjusted daily (Appendix B8; unpublished data of Conklin and Neilson, 2005). The actual amount of water allowed to percolate is the lesser of the calculated flux from a given layer (layer 1 or 2) or the available water-holding capacity ($W_{fi} \times Depth_{(n)} - pool_{w(n)}$) in the layer below (layer 2 or 3). Percolated water from soil layer 3 is immediately removed as runoff.

A6. Evapotranspiration (Computed daily)

The potential evaporation (ev_{pm}) and transpiration (tr_{pm}) are estimated by the Penman–Monteith method (Monteith and Unsworth, 1990), assuming an abundant water supply:

$$ev_{pm} = dlen \times \frac{0.5 \times slope_{vps} \times radnet_{soil} + 1012 \times dnsa \times vpd \times c_{aero}}{695\{slope_{vps} + 0.667(1.0 + c_{aero}/c_{soil})\}}, \tag{A44}$$

$$tr_{pm} = dlen \times \frac{0.5 \times slope_{vps} \times radnet_{veg} + 1012 \times dnsa \times vpd \times c_{aero}}{695\{slope_{vps} + 0.667(1.0 + c_{aero}/c_{leaf})\}} - ic, \tag{A45}$$

where $0.5 \times radnet_{veg}$ is the daily average of net radiation at vegetation when daily change of radiation was approximated by $\sin^2$. The constant 1012 is the specific heat of air (in J kg^{-1} K^{-1}), 695 is the latent heat of vaporization (in Wh kg^{-1} H_2O), and 0.667 is the psychrometer constant (in hPa K^{-1}); c_{aero}, c_{soil}, and c_{leaf} are aerodynamic conductance, soil surface

conductance, and canopy conductance, respectively; c_{aero}, aerodynamic conductance is proportional to wind velocity:

$$c_{aero} = \frac{0.41^2 \times wind}{[\log(\alpha)]^2}, \quad \text{(A46)}$$

where 0.41 is Von Karman's constant and *wind* is the wind velocity (m/s) at 10m height. We assigned vegetation specific constant α a value of 17.4 for forest biome and 146.0 for other biome. c_{soil}, soil surface conductance, is in proportion to the fraction of soil layer 1 that is saturated with water:

$$c_{soil} = 0.0224 \times \min\left[\left(\frac{pool_{w(1)}}{Wfi \times Depth_{(1)}}\right)^2, 1\right], \quad \text{(A47)}$$

where the multiplier 0.0224 is water-saturation conductance. Finally, c_{leaf} is

$$c_{leaf} = 0.0224 \times ccon, \quad \text{(A48)}$$

where the multiplier 0.0224 is the unit converter from [mol H_2O m^{-2} s^{-1}] to [m^3 H_2O m^{-2} s^{-1}].

Due to the limited water availability, evapotranspiration rates were reduced from their potential values, ev_{pm} and tr_{pm}, to their actual values, *ev* and *tr*, as approximated by the quadratic functions:

$$0.1\,ev^2 - (a + ev_{pm})\,ev + a \times ev_{pm} = 0, \tag{A49}$$

$$0.1\,tr^2 - (b + tr_{pm})\,tr + b \times tr_{pm} = 0, \tag{A50}$$

where 0.1 is the empirical convexity of the available water to the actual evapotranspiration curves; a and b are available water for evaporation and transpiration, respectively; $a = pool_{w(1)}$, $b = \max(0, pool_{w(1)} - Depth_{(1)} \times Wwilt) + \max(0, pool_{w(2)} - Depth_{(2)} \times Wwilt)$. These equations can be transformed as follows:

$$ev = \frac{(a + ev_{pm}) - \sqrt{(a + ev_{pm})^2 - 4 \times 0.1 \times a \times ev_{pm}}}{2 \times 0.1}, \tag{A51}$$

$$tr = \frac{(b + tr_{pm}) - \sqrt{(b + tr_{pm})^2 - 4 \times 0.1 \times b \times tr_{pm}}}{2 \times 0.1}, \tag{A52}$$

Actual evaporation, ev, is charged only for soil layer 1. Actual transpiration, tr, is charged for soil layers 1 and 2 in proportion to the soil wetness of each layer.

Appendix B

B1. Inputs and outputs of the SEIB–DGVM

Input

(1) Location

latitude, altitude

(2) Soil (fixed in time)

soil moisture at saturation point, field capacity, matrix potential, wilting point, albedo

(3) Climatic data (daily)

air temperature, soil temperature, fraction of cloud cover, precipitation, humidity, wind velocity

Outputs

(1) Carbon dynamics (daily–yearly)

terrestrial carbon pool (woody biomass, grass biomass, litter, soil organic matter), CO2 absorption and emission rates

(2) Water dynamics (daily)

soil moisture content (three layers), interception rate, evaporation rate, transpiration rate, interception rate, runoff rate

(3) Radiation (daily)

albedo from terrestrial surface

(4) Properties of vegetation (daily–yearly)

vegetation type, dominant plant functional type, leaf area index, tree density, size distribution of trees, age distribution of trees, woody biomass for each tree, grass biomass per unit area

B2. Processes in the SEIB–DGVM, and the approaches used to represent each process

Process	Approach	Source
Physical process		
Radiation	Beer's Law within spatially explicit virtual forest	
Evapotranspiration	Penman–Monteith evapotranspiration	Monteith and Unsworth (1990)
Soil water process	Empirical analogs of Darcy's law: saturated and unsaturated percolation in three soil layers	Neilson (1995)
Physiology		
Photosynthesis	Michaelis-type function	
Maintenance respiration	The respiration rate is in proportion to the nitrate content of each organ.	Ryan (1991)
Growth respiration	The respiration rate is based on the chemical composition of each organ.	Poorter (1994)
Stomatal conductance	A semiempirical model	Ball et al. (1987) modified by Leuning (1995)
Phenology	A set of semiempirical models; parameters were estimated from satellite NDVI data.	Botta et al. (2000)
Decomposition	Three carbon sources: litter and soil organic carbon with slow and fast decomposition rates	Foley (1995) and Lloyd and Taylor (1994)
Vegetation dynamics		
Establishment	Climatically favored PFTs establish as small individuals.	
Mortality	Annual NPP per leaf area, heat stress, bioclimatic limit, and fire	Sitch et al. (2003)
Disturbance	Fire as an empirical function of soil moisture and aboveground biomass	Kistler et al. (2001)

B3. Parameters and constants in the model's equations

Fixed parameters (begins with a capital letter)

Soil properties (Grid specific)

W_{sat} : soil moisture at saturation point (m m^{-1})

W_{fi} : soil moisture at field capacity (m m^{-1})

W_{mat} : soil moisture at matrix potential (m m^{-1})

W_{wilt} : soil moisture at wilting point (m m^{-1})

ALBEDO : soil albedo (fraction)

$Depth_{(n)}$: depth of soil layer *n* (mm)

Soil properties (Global value)

$K_{u1(n)}$, $K_{u2(n)}$: percolation coefficients of unsaturated soil of soil layer *n* (dimensionless)

$K_{s1(n)}$, $K_{s2(n)}$: percolation coefficients of saturated soil of soil layer *n* (dimensionless)

Location

LAT : latitude (degree)

ALT : altitude (m)

Allocation and Allometry (PFT-specific)

HGTmax : maximum tree height (m)

HGTs : initial value of relative growth rate, height to diameter (m m^{-1})

LAmax : maximum leaf area per canopy surface (m^2 m^{-2})

CDmax : maximum crown diameter (m)

SLA : specific leaf area (one sided m^2 g DM^{-1})

P_{root} : proportion of root mass in soil layer 1 (varying 0.0–1.0)

$ALM_{1, 2, 4}$: allometric parameter 1, 2, 4 (dimensionless)

ALM_3 : allometric parameter 3 (g DM m^{-3})

FRratio : ratio of foliage mass to fine root mass (ratio)

Respiration and turnover (PFT-specific)

$PN_{f, s, r}$:nitrogen mass per biomass for foliage, sapwood, root (g N g DM^{-1})

RM :maintenance respiration rate at 15°C for unit nitrogen mass (g C g N^{-1} day^{-1})

$RG_{f, s, r}$:specific growth respiration rate for foliage, sapwood, and root (g DM g DM^{-1})

$RG_{stockin}$:growth respiration rate from available resource to stock resource (g DM g DM^{-1})

$RG_{stockout}$:growth respiration rate from stock resource to available resource (g DM g DM^{-1})

$TO_{f, s, r}$:turnover rate for foliage, sapwood, and root (DM^{-1} $year^{-1}$)

$TO_{fast, slow}$:turnover rates for fast and slow soil organic matter (SOM) (DM^{-1} yr^{-1})

Photosynthesis (PFT-specific)

PMAX : maximum photosynthesis rate (μmol mol^{-1} CO_2 m^{-2} s^{-1})

EK : light attenuation coefficient for vertical direction (dimensionless)

LUE : control value of light-use efficiency for photosynthesis (mol CO_2 mol $photon^{-1}$)

T_{opt0} :optimum temperature for photosynthesis at very low intercellular CO_2 concentration (°C)

T_{min} : minimum temperature for photosynthesis (ºC)

T_{max} : maximum temperature for photosynthesis (ºC)

GS_{b1} : parameters for stomatal conductance (mol H_2O m^{-2} s^{-1})

GS_{b2} : parameters for stomatal conductance (dimensionless)

GS_{b3} : parameters for stomatal conductance (hPa)

KM : dependence of photosynthesis on intercellular CO_2 concentration (μmol mol^{-1})

$CO2cmp$: CO_2 compensation point at 20°C (μmol CO_2 mol^{-1} air)

Establishment (PFT-specific)

$P_{establish}$: establishment probability at vacant patch (m^{-2} $year^{-1}$)

$GDDmin$: minimum growth-degree-day sum (5 ºC base)

TC_{max} : maximum coldest-month temperature (ºC)

Mortality (PFT-specific)

M_1 : parameter for background mortality (dimensionless)

M_2 : parameter for background mortality (dimensionless)

M_3 : probability of survival after fire (varying 0.0–1.0)

TC_{min} : minimum coldest-month temperature for survival (ºC)

Other fixed parameters

ESD : distance between sun and earth (km)

ESD_{mean} : annual mean of ESD (km)

Variables (Begins with a lowercase letter)

Daily climatic data

tmp_{air} : air temperature (ºC)

tmp_{soil} : soil temperature at 10 cm depth (ºC)

cloud : total cloud cover (fraction)

prec : daily precipitation (mm day^{-1})

humid : air humidity (g g^{-1})

wind : wind velocity (m s^{-1})

Woody biomass (for each individual tree)

$mass_{leaf}$: leaf biomass (g DM)

$mass_{trunk}$: trunk biomass (g DM)

$mass_{root}$: fine root biomass (g DM)

$mass_{stock}$: stock biomass (g DM)

$mass_{available}$: available biomass (g DM)

Grass biomass

$gmass_{leaf}$: leaf biomass density of grass (g DM m^{-2})

$gmass_{root}$: root biomass density of grass (g DM m^{-2})

$gmass_{stock}$: stock biomass density of grass (g DM m^{-2})

$gmass_{available}$: available biomass density of grass (g DM m^{-2})

Morphology and characteristics for woody PFTs (for each individual tree)

height : tree height (m)

$crown_{diameter}$: crown diameter (m)

$crown_{depth}$: crown depth (m)

$crown_{area}$: cross sectional crown area (m^2)

$dbh_{sapwood}$: sapwood diameter (m)

$dbh_{heartwood}$: heartwood diameter (m)

la : leaf area (m^2)

la_{mean} : annual mean leaf area in the previous year (m^2)

Photosynthesis conditions

p_{top} : midday photosynthetic rates at top of the leaf layer ($\mu mol\ CO_2\ m^{-2}\ s^{-1}$)

p_{sat} : light saturated photosynthetic rate ($\mu CO_2\ m^{-2}\ s^{-1}$)

lue : light-use efficiency of photosynthesis (mol CO_2 mol $photon^{-1}$)

$co2_{cmp}$: CO_2 compensation point (μmol CO_2 mol air^{-1})

$co2_{cell}$: intercellular CO_2 concentration (μmol CO_2 mol air^{-1})

t_{opt} : optimum temperature for photosynthesis (ºC)

gs_{top} : midday leaf stomatal conductance of H_2O on top of the leaf layer (mol $CO_2\ m^{-2}\ s^{-1}$)

gs : midday leaf stomatal conductance of H_2O (mol $CO_2\ m^{-2}\ s^{-1}$)

gs_{top} : midday leaf stomatal conductance of H_2O on top of the leaf-layer (mol $CO_2\ m^{-2}\ s^{-1}$)

$ccon_{wood}$: stomatal conductance of H_2O of tree canopy, day time mean (mol $H_2O\ m^{-2}\ s^{-1}$)

$ccon_{grass}$: stomatal conductance of H_2O of grass leaves, day time mean (mol $H_2O\ m^{-2}\ s^{-1}$)

ccon : stomatal conductance of H_2O, day time mean (=$ccon_{wood}$+ $ccon_{grass}$, mol H_2O m^{-2} s^{-1})

Production

gpp : gross primary production of each tree (g DM day^{-1})

gpp_l : gross primary production of each crown layer (g DM day^{-1})

gpp_g : gross primary production of grass layer (g DM day^{-1} m^{-2})

anpp : annul net primary production of the previous year (kg DM $year^{-1}$)

$stat_{leaf}$: benefit per cost of maintaining leaf mass (g g^{-1} day^{-1})

Other metabolic variables

lai : leaf area index of each PFT (m^2 m^{-2})

lai_g : leaf area index of grass layer (m^2 m^{-2})

$stat_{water}$: state of water availability for each PFT (varying 0.0–1.0)

qt : temperature sensitivity of respiration (dimensionless)

Soil water cycle

$prec_{rain}$: precipitation, rain (mm day^{-1})

$prec_{snow}$: precipitation, snow (mm day^{-1})

rain : expected number of rain in a day (day^{-1})

$pool_{w(n)}$: water content at soil layer *n* (mm)

$pool_{snow}$: water-equivalent snow depth (mm)

tw : snowmelt rate (mm day^{-1})

$pn_{(n)}$: penetration rate for soil layer *n* (mm day^{-1})

ev : actual evaporation rate from soil layer 1 (mm day^{-1})

ev_{pm} : potential evaporation rate from soil layer 1 (mm day^{-1})

$tr_{(n)}$: actual transpiration rate from soil layer n (mm day^{-1})

tr_{pm} : potential transpiration rate (mm day^{-1})

ic : intercepted rainfall by plants (mm day^{-1})

aet : actual evapotranspiration of the previous year (mm $year^{-1}$)

c_{aero} : aerodynamic conductance of evaporation (dimensionless)

c_{soil} : soil conductance of evapotranspiration (dimensionless)

c_{leaf} : canopy conductance of transpiration (dimensionless)

Radiation conditions at midday

rad_{intact} : shortwave radiation at top of atmosphere (W m^{-2})

rad : shortwave radiation entering biosphere (W m^{-2})

rad_{direct} : direct radiation within rad (W m^{-2})

$rad_{diffuse}$: diffused radiation within rad (W m^{-2})

$radnet_{veg}$: net radiation at vegetation surface (W m^{-2})

$radnet_{soil}$: net radiation at soil surface (W m^{-2})

$radnet_{long}$: net long wave radiation (W m^{-2})

par : midday PAR (μmol photon m^{-2} s^{-1})

par_{direct} : direct radiation component of par (μmol photon m^{-2} s^{-1})

$par_{diffuse}$: diffused radiation component of par (μmol photon m^{-2} s^{-1})

$par_{wood\ (l,\ n)}$: midday PAR on crown layer l of individual tree n (μmol photon m^{-2} s^{-1})

par_{grass} : midday PAR at the grass layer (μmol photon m^{-2} s^{-1})

$fpar_{direct(l,\ n)}$: relative intensity of direct PAR of crown disk l of tree n at midday

compared to the forest top (dimensionless)

$fpar_{diffuse(l)}$: relative intensity of diffused of forest layer l at midday compared to the forest top (dimensionless)

$fpar_{direct}$:relative intensity of direct PAR of crown disk l of tree n at midday compared to the forest top (dimensionless)

sl_{hgt} : solar angle at midday (degree)

sl_{dec} : solar declination of the Earth's orbit (degree)

dlen : day length (hour)

eK : light attenuation coefficient at midday (dimensionless)

ir : shortwave interception by leaves (fraction)

$albedo_{veg}$: albedo of vegetation surface (fraction)

$albedo_{soil}$: albedo of soil surface (fraction)

Air characteristics

ap : air pressure (hPa)

vp : actual vapor pressure (hPa)

vp_{sat} : saturated vapor pressure (hPa)

vpd : vapor pressure deficit between saturated and actual vapor pressures (hPa)

co2atm : ambient (canopy) CO_2 concentration (μmol CO_2 mol^{-1} air)

$slope_{vps}$: slope of saturated vapor pressure (hPa $ºC^{-1}$)

dnsa : density of air (kg m^{-3})

1 B4. PFT-specific allocation and allometric parameters

PFT	ALM_1	ALM_2	ALM_3	ALM_4	$HGTmax$	$HGTs$	$FRratio$	SLA	$LAmax$	$CDmax$
	-	-	(g DM m^{-3})	-	(m)	(m m^{-1})	(ratio)	(m^2 g^{-1})	(m^2 m^{-2})	(m)
TrBE	7000	200	492000	0.50	76.5	165.0	1.50	0.010	5.0	30.0
TrBR	7000	200	492000	0.50	35.0	150.0	1.50	0.013	5.0	15.0
TeNE	4800	100	374000	0.38	43.0	65.0	1.50	0.004	4.0	15.0
TeBE	4800	200	492000	0.38	17.0	154.3	1.50	0.007	4.0	15.0
TeBS	14500	200	492000	0.20	37.0	159.0	1.50	0.015	2.0	15.0
BoNE	6000	100	374000	0.20	35.0	130.0	1.50	0.004	2.0	10.0
BoNS	6000	100	287700	0.20	28.3	164.3	1.50	0.015	2.0	10.0
BoBS	8500	200	492000	0.30	35.0	200.0	1.50	0.016	4.0	10.0
TeH	-	-	-	-	-	-	1.00	0.020	-	-
TrH	-	-	-	-	-	-	1.00	0.015	-	-

2

1 B5. PFT-specific dynamic parameters

PFT	M_1 (no dimension)	M_2 (no dimension)	M_3 (no dimension)	$P_{establish}$ (m^{-2} $year^{-1}$)	TC_{min} (ºC)	TC_{max} (ºC)	$GDDmin$ (5 ºC base)
TrBE	0.015	1.5	0.12	0.015	15.5	-	-
TrBR	0.015	1.5	0.50	0.015	15.5	-	-
TeNE	0.018	1.0	0.12	0.040	-2.0	22.0	900
TeBE	0.018	1.0	0.50	0.040	3.0	18.8	1200
TeBS	0.010	2.5	0.12	0.013	-17.0	15.5	1200
BoNE	0.013	1.2	0.12	0.005	-32.5	-2.0	600
BoNS	0.013	1.2	0.12	0.005	-	-2.0	350
BoBS	0.015	2.0	0.12	0.020	-	-2.0	350

2

1 B6. PFT-specific respiration and turnover parameters

PFT	RM (gC gN^{-1} day^{-1})	PN_f (gN gDM^{-1})	RG_f (gDM gDM^{-1})	RG_s (gDM gDM^{-1})	RG_r (gDM gDM^{-1})	$RG_{stockin}$ (gDM gDM^{-1})	$RG_{stockout}$ (gDM gDM^{-1})	TO_f (year^{-1})	TO_s (year^{-1})	TO_r (year^{-1})
TrBE	0.1	0.016	1.56	1.68	1.34	1.10	1.10	0.59	0.05	0.76
TrBR	0.1	0.022	1.56	1.68	1.34	1.10	1.10	1.59	0.05	0.76
TeNE	0.1	0.012	1.56	1.68	1.34	1.10	1.10	0.22	0.05	0.64
TeBE	0.1	0.012	1.56	1.68	1.34	1.10	1.10	0.38	0.05	0.64
TeBS	0.1	0.022	1.56	1.68	1.34	1.10	1.10	2.17	0.05	0.64
BoNE	0.1	0.012	1.56	1.68	1.34	1.10	1.10	0.22	0.05	0.42
BoNS	0.1	0.026	1.56	1.68	1.34	1.10	1.10	4.00	0.05	0.42
BoBS	0.1	0.025	1.56	1.68	1.34	1.10	1.10	3.33	0.05	0.42
TeH	0.1	0.027	1.50	-	1.34	1.10	1.10	3.19	-	0.40
TrH	0.1	0.018	1.50	-	1.34	1.10	1.10	6.70	-	0.90

2

1 B7. PFT-specific photosynthesis parameters

PFT	*PMAX* (µmol mol^{-1} CO_2 m^{-2} s^{-1})	*EK* no dimension	*LUE* (mol CO_2 mol $photon^{-1}$)	T_{opt0} (C °)	T_{min} (C °)	T_{max} (C °)	GS_{b1} (mol H_2O m^{-2} s^{-1})	GS_{b2} no dimension	GS_{b3} (hPa)	*KM* (µmol mol^{-1})	*CO2cmp* (µmol CO_2 mol^{-1} air)
TrBE	5.0	0.50	0.05	27.5	2.0	47.5	0.01	20.0	100.0	33.0	50.0
TrBR	5.0	0.50	0.05	27.5	2.0	47.5	0.01	20.0	100.0	30.0	50.0
TeNE	4.0	0.50	0.05	25.0	0.0	45.0	0.01	20.0	100.0	30.0	50.0
TeBE	4.0	0.50	0.05	25.0	0.0	45.0	0.01	20.0	100.0	30.0	50.0
TeBS	7.0	0.50	0.05	22.5	-2.0	42.5	0.01	20.0	100.0	30.0	50.0
BoNE	5.2	0.50	0.05	18.0	-4.0	38.5	0.01	20.0	100.0	30.0	50.0
BoNS	6.0	0.50	0.05	18.0	-4.0	38.5	0.01	20.0	100.0	35.0	50.0
BoBS	6.0	0.50	0.05	18.0	-4.0	38.5	0.01	20.0	100.0	35.0	50.0
TeH	8.0	0.50	0.05	-	-1.0	45.0	0.01	10.0	100.0	37.0	50.0
TrH	12.0	0.50	0.05	-	2.5	55.0	0.01	5.0	100.0	10.0	5.0

2

1 B8. Soil percolation parameters for each soil layer (dimensionless)

Soil layer	K_{1u}	K_{2u}	K_{1s}	K_{2s}
1	0.80	2.5	0.30	2.0
2	0.15	3.0	0.30	3.0
3	0.01	10.0	0.30	10.0

2

B9. Classification scheme of vegetation type, taken from Haxeltine and Prentice (1996) with some simplifications.

Vegetation type conditions	Dominant PFT	Other
Group 1		
Desert (polar)	any	$GDD_0 < 150$
Group 2		
Arctic / Alpine-tundra	any	$GDD_5 < 350$
Group 3		
Tropical forest	TrBE	$2.5 \leq LAI_{max}$
Tropical deciduous forest	TrBR	$2.5 \leq LAI_{max}$
Temperate evergreen forest	TeNE	$1.5 \leq LAI_{max}$
Temperate evergreen forest	TeBE	$3.0 \leq LAI_{max}$
Temperate deciduous forest	TeBS	$2.5 \leq LAI_{max}$
Boreal evergreen forest	BoNE	
Boreal deciduous forest	BoNS or BoBS	
Group 4		
Xeric wood-land / scrub	Tropical woody or TeBE	$1.0 \leq LAI_{max}$
	Boreal woody or TeNE or TeBS	$1.5 \leq LAI_{max}$
Group 5		
Grass land / Savannas / Steppe	any	$0.2 \leq LAI_{max}$
Desert (arid)	any	$LAI_{max} < 0.2$

Priority of classification: Group 1 > Group 2 > Group 3 > Group 4 > Group 5
GDD_0 : growing-degree-day at 0 °C base
GDD_5 : growing-degree-day at 5 °C base
LAI_{max} : maximum leaf area index of the previous year ($m^2\ m^{-2}$)

Acknowledgments

We sincerely thank Taro Matsuno, Michio Kawamiya, Tomomichi Kato, Rikie Suzuki, Eitaro Wada, Takuya Kubo, and all members of the Kyousei 2 Project (Category 2 of the Research Project for Sustainable Coexistence of Human, Nature, and the Earth) for suggestions and encouragement. Koji Ohgochi assisted with the mass computation. Martin Sykes and Ian Wright shared personal data. Dave Conklin and Ronald Neilson provided recalibrated parameters for the soil hydrological processes. Sven E Jørgensen and an anonymous reviewer gave us valuanle comments on the manuscripts. Data on forest dynamics used in this paper were obtained from scientists participating in PlotNet, the forest dynamics database of FFPRI, and the Hubbard Ecosystem Study (operated and maintained by the Northeastern Research Station, USA); these scientists have not reviewed this paper.

Literature cited

Arora, V., 2002. Modeling vegetation as a dynamic component in soil-vegetation-atmosphere transfer schemes and hydrological models. Rev. Geophys. 40, 1006, doi:10.1029/2001RG000103.

Arora, V.K., Boer, G..J., 2005. A parameterization of leaf phenology for the terrestrial ecosystem component of climate models. Global Change Biol. 11, 39–59.

Ball, J.T., Woodrow, I.E., Berry, J.A., 1987. A model predicting stomatal conductance and its contribution to the control of photosynthesis under different environmental conditions. In: Biggens, J. (Eds.), Progress in Photosynthesis Research. Martinus Nijhoff Publishers, Dordrecht, pp. 221–224.

Botta, A., Viovy, N., Ciais, P., Friedlingstein, P., Monfray, P., 2000. A global prognostic scheme of leaf onset using satellite. Global Change Biol. 6, 709–725.

Brooks, A., Farquhar, G.D., 1985. Effect of temperature on the CO_2/O_2 specificity of ribulose 1,5-bisphosphate carboxylase/oxygenase and the rate of respiration in the light, Estimates from gas-exchange measurements on spinach. Planta 165, 397–406.

Bugmann, H., 2001. A review of forest gap models. Clim. Change 51, 259–305.

Cox, P.M., 2001. Description of the "TRIFFID" Dynamic GLobal Vegetation Model. Hadley Centre technical note 24, 1–16.

Cox, P.M., Betts, R.A., Jones, C.D., Spall, S.A., Totterdell, I.J., 2000. Acceleration of global warming due to carbon-cycle feedbacks in a coupled climate model. Nature 408, 184–187.

Cramer, W., Bondeau, A., Woodward, F.I., Prentice, I.C., Betts, R.A., Brovkin, V., Cox, P.M., Fisher, V., Foley, J.A., Friend, A.D., Kucharik, C., Lomas, M.R., Ramankutty, N., Sitch, S., Smith, B., White, A., Young-Molling, C., 2001. Global response of terrestrial ecosystem structure and function to CO_2 and climate change: results from six dynamic global vegetation models. Global Change Biol 7, 357–373.

Farquhar, G.D., von Caemmerer, S., 1982. Modelling of photosynthetic response to environmental conditions. In: Nobel, P.S., Osmond, C.B., Ziegler, H. (Eds.), Physiological Plant Ecology II: Water Relations and Carbon Assimilation. Springer, Berlin, pp. 549–587.

Farquhar, G.D., von Caemmerer, S., Berry J.A., 1980. A biochemical model of photosynthetic CO_2 assimilation in leaves of C3 plants. Planta 149, 78–90.

FFPRI (Forestry and Forest Products Research Institute), 1982. Properties of timber. In: The handbook of wood industries, 3rd eds (in Japanese). Maruzen Publishers, Tokyo, pp. 62–63.

FFPRI (Forestry and Forest Products Research Institute), Viewed October 27 2004, 2003. Forest Dynamics Database (http://fddb.ffpri-108.affrc.go.jp/).

Foley, J.A., 1995. An equilibrium model of the terrestrial carbon budget. Tellus, Ser. B 47, 310–319.

Foley, J.A., Costa, M.H., Delire, C., Ramankutty, N., Snyder, P., 2003. Green surprise? How terrestrial ecosystems could affect earth's climate. Frontier Ecol. Environ. 1, 38–44.

Friend, A.D., Stevens, A.K., Knox, R.G., Cannell, M.G.R., 1997. A process-based, terrestrial biosphere model of ecosystem dynamics (Hybrid v3.0). Ecol. Modell. 95, 249–287.

Gill, R.A., Jackson, R.B., 2000. Global patterns of root turnover for terrestrial ecosystems. New Phytol. 147, 13–31.

Greene, D.F., Zasada, J.C., Sirois, L., Kneeshaw, D., Morin, H., Charron, I., Simard, M.-J., 1999. A review of the regeneration dynamics of North American boreal forest tree species. Can. J. For. Res. 29, 824–839.

Haxeltine, A., Prentice, I.C., 1996. BIOME3: An equilibrium terrestrial biosphere model based on ecophysiological constrains, resource availability, and competition among plant functional types. Global Biogeochem. Cycles 10, 693–709.

Hillel, D., 1982. Introduction to soil physics. Academic Press, NewYork, USA.

Ito, A., Oikawa, T., 2002. A simulation model of the carbon cycle in land ecosystems (Sim-CYCLE): a description based on dry-matter production theory and plot-scale validation. Ecol. Modell. 151, 143–176.

Joos, F., Prentice, I.C., Sitch, S., Meyer, R., Hooss, G., Plattner, G., Gerber, S., Hasselmann, K., 2001. Global warming feedbacks on terrestrial carbon uptake under the Intergovernmental Panel on Climate Change (IPCC) emission scenarios. Global Biogeochem. Cycles 15, 891–907.

Jones, H. G., 1992. Radiation. In: Plants and microclimate, 2nd ed, pp:9–44, Cambridge University press.

Kira, T., Shidei, T., 1967. Primary production and turnover of organic matter in different forest ecosystems of the western Pacific. Jpn. J. Ecol. 17, 70–87.

Kistler, R., Kalnay, E., Collins, W., Saha, S., White, G., Woollen, J., Chelliah, M., Ebisuzaki, W., Kanamitsu, M., Kousky, V., van den Dool, H., Jenne, R., Fiorino, M., 2001. The NCEP-NCAR 50-year reanalysis: monthly means CD-ROM and documentation. Bull. Am. Meteorol. Soc. 82, 247–267.

Kohyama, T., Shigesada, N., 1995. A size-distribution-based model of forest dynamics along a latitudinal environmental gradient. Vegetatio 121, 117–126.

Kohyama, T., Suzuki, E., Aiba, S., Seino, T., 1999. Functional differentiation and positive feedback enhancing plant biodiversity. In: Kato, M. (Eds.), Biology of Biodiversity. Springer, Tokyo, pp. 179–191.

Kohyama, T., 2005. Scaling up from shifting-gap mosaic to geographic distribution in the modeling of forest dynamics. Ecol. Res. 20, 305–312.

Köppen, W., 1936. Das Geographische System der Klimate. In: Köppen, W. and Geiger, R. (Eds.), Handbuch der Klimatologie. Gebruder Borntraeger, Berlin, pp. C1–C44.

Krinner, G., Viovy, N., de Noblet-Ducoudre, N., Ogee, J., Polcher, J., Friedlingstein, P., Ciais, P., Sitch, S., Prentice, I.C., 2005. A dynamic global vegetation model for studies of the coupled atmosphere-biosphere system. Global Biogeochemical Cycles 19, GB1015.

Kucharik, C.J., Foley, J.A., Delire, C., Fisher, V.A., Coe, M.T., Lenters, J.D., Young-Molling, C., Ramankutty, N., Norman, J.M., Gower, S.T., 2000. Testing the performance of a Dynamic Global Ecosystem Model: Water balance, carbon balance, and vegetation structure. Global Biogeochemical Cycles 14, 795–825.

Kuroiwa, S., 1979. Population photosynthesis. In: Iwajyo, H. (Eds.), Function and productivity of plant population (in Japanese). Asakura-shoten, Tokyo, pp. 84–141.

Lambers, H., Chapin III, F.S., Pons, T.L., 1998. Plant Physiological Ecology. Springer, New-York.

Larcher, W., 1995. Ecophysiology and stress physiology of functional groups. In: Physical plant ecology. Springer, Berlin, p. 506.

Leuning, R., 1995. A critical appraisal of a combined stomatal-photosynthesis model for C_3 plants. Plant Cell Environ. 18, 339–355.

Lloyd, J., Taylor, J.A., 1994. On the temperature dependence of soil respiration. Func. Ecol. 8, 315–323.

Monteith, J.L., Unsworth, M.H., 1990. Principles of Environmental Physics. 2nd edition. Arnold Press, London.

Neilson, R.P., 1995. A model for predicting continental-scale vegetation distribution and water balance. Ecol. Appl. 5, 362–385.

Osmond, C.B., Björkman, O., Anderson, D.J., 1980. Photosynthesis. In: Physiological Processes in Plant Ecology. Springer-Verlag, Berlin, pp. 291–377.

Pacala, S.W., Deutschman, D.H., 1995. Details that matter: The spatial distribution of individual trees maintains forest ecosystem function. Oikos 74, 357–365.

Peng, C.H., 2000. From static biogeographical model to dynamic global vegetation model: a global perspective on modelling vegetation dynamics. Ecol. Modell. 135, 33–54.

Penning de Vries, F.W.T., 1975. Use of assimilates in higher plants. In: Cooper, J.P. (Eds.), Photosynthesis and productivity in different environments. Cambridge Univ. Press, pp. 459–480.

Pitman, A.J., 2003. The evolution of, and revolution in, land surface schemes designed for climate models. International Journal of Climatology 23, 479–510.

Poorter, H., 1994. Construction costs and payback time of biomass: A whole plant perspective. In: Roy, J., Garnier, E. (Eds.), A whole plant perspective on carbon-nitrogen interactions. SPB Academic Publishing, Hague, Netherlands, pp. 111–127.

Pregitzer, K.S., Euskirchen, E.S., 2004. Carbon cycling and storage in world forests: biome patterns related to forest age. Global Change Biol. 10, 2052–2077.

Raich, J.W., Rastetter, E.B., Melillo, J.M., Kicklighter, D.W., Steudler, P.A., Peterson, B.J., Grace, A.L., Moore III, B., Vörösmarty, C.J., 1991. Potential net primary productivity in South America: application of a global model. Ecol. Appl. 1, 399–429.

Reich, P.B., Walters, M.B., Ellsworth, D.S., 1997. From tropics to tundra: Global convergence in plant functioning. Proc. Natl. Acad. Sc. USA 94, 13730–13734.

Ryan, M.G., 1991. Effects of cllimate change on plant respiration. Ecol. Appl. 1, 157–167.

Sala, O.E., 2001, Productivity of temperate grasslands. In: Roy, J., Saugier, B., Mooney, H.A. (Eds.), Terrestrial Global Productivity. Academic Press, pp. 285–300.

Schulze, E.-D., Schulze, W., Kelliher, F.M., Vygodskaya, N.N., Ziegler, W., Kobak, K.I., Koch, H., Arneth, A., Kusnetsova, W.A., Sogatchev, A., Issajev, A., Bauer, G., Hollinger , D.Y., 1995. Aboveground biomass and nitrogen nutrition in a chronosequence of pristine Dahurian *Larix* stands in eastern Siberia. Can. J. For. Res. 25, 943–960.

Shinozaki, K., Yoda, K., Hozumi, K., Kira, T., 1964a. A quantitative analysis of plant form — The pipe model theory I. Jpn. J. Ecol. 14, 97–105.

Shinozaki, K., Yoda, K., Hozumi, K., Kira, T., 1964b. A quantitative analysis of plant form — The pipe model theory II: Further evidence of the theory and its application in forest ecology, Jpn. J. Ecol. 14, 133–139.

Sitch, S., Smith, B., Prentice, I.C., Arneth, A., Bondeau, A., Cramer, W., Kaplan, J.O., Levis, S., Lucht, W., Sykes, M.T., Thonicke, K., Venevski, S., 2003. Evaluation of ecosystem dynamics, plant geography and terrestrial carbon cycling in the LPJ dynamic global vegetation model. Global Change Biol. 9, 161–185.

Smith, B., Prentice, I.C., Sykes, M.T., 2001. Representation of vegetation dynamics in the modelling of terrestrial ecosystems: comparing two contrasting approaches within European climate space. Global Ecology and Biogeography 10, 621–637.

Starfield, A.M., Chapin III, F.S., 1996. Model of transient changes in arctic and boreal vegetation in response to climate and land use change. Ecol. Appl. 6, 842–864.

Takahashi, K., Homma, K., Vetrova, V.P., Florenzev, S., Hara, T., 2001. Stand structure and regeneration in a Kamchatka mixed boreal forest. Journal of vegetation science 12, 627–634.

Takenaka, A., 2005. Local coexistence of tree species and the dynamics of global distribution pattern along an environmental gradient: a simulation study. Ecol. Res. 20, 297–304.

Thonicke, K., Venevsky, S., Sitch, S., Cramer, W., 2001. The role of fire disturbance for global vegetation dynamics: coupling fire into a Dynamic Global Vegetation Model. Global Ecology and Biogeography 10, 661–677.

Warning, R.H., 1983. Estimating forest growth and efficiency in relation to canopy leaf area. Adv. Ecol. Res. 13, 327–354.

Woodward, F.I., Lomas, M.R., 2004. Vegetation dynamics – simulating responses to climatic change. Biol. Rev. 79, 643–670.

Woodward, F.I., Lomas, M.R., Betts, R.A., 1998. Vegetation-climate feedbacks in a greenhouse world. Phil. Trans. R. Soc. Land. B 353, 29–39.

Woodward, F.I., Smith, T.M., Emanuel, W.R., 1995. A global land primary productivity and phytogeography model. Global Biogeochem. Cycles 9, 471–490.

Wright, I.J., Reich, P.B., Westoby, M., Ackerly, D.D., Baruch, Z., Bongers, F., Cavender-Bares, J., Chapin, T., Cornelissen, J.H.C., Diemer, M., Flexas, J., Garnier, E., Groom, P.K., Gulias, J., Hikosaka, K., Lamont, B.B., Lee, T., Lee, W., Lusk, C., Midgley, J.J., Navas, M., Niinemets,

U., Oleksyn, J., Osada, N., Poorter, H., Poot, P., Prior, L., Pyankov, V.I., Roumet, C., Thomas, S.C., Tjoelker, M.G., Veneklaas, E.J., Villar, R., 2004. The worldwide leaf economics spectrum. Nature 428, 821–827.

Yokota, T., Hagihara, A., 1996. Seasonal change in the temperature coefficient Q10 for respiration of field-grown hinoki cypress (Chamaecyparis obtusa) trees. Journal of Forest Research 1, 165–168.

Zeide, B., 2001. Natural thinning and environmental change: an ecological process model. Forest Ecology and Management 154, 165–177.

Figure captions

Figure 1

Representation of individual trees in the SEIB–DGVM. Each tree is composed of a crown, trunk, and fine roots. The trunk is composed of heartwood and sapwood. Trunk biomass includes branches and coarse/tap roots. The crown consists of 10-cm-deep 'disks'. The trunk and the crown both have cylindrical shapes, while the fine roots are formless (i.e., represented only by biomass).

Figure 2

The carbon flow through a terrestrial ecosystem as simulated by the SEIB–DGVM.

Figure 3

The water flow through the terrestrial ecosystem as simulated by the SEIB–DGVM.

Figure 4

Schematic diagram of how to allocate direct radiation among trees in the SEIB–DGVM.

Figure 5

Relationships between annual precipitation and aboveground net-primary-production. The broken line represents the regression from field observations in the U.S. central plains, while solid line is the simulated results in the Central Plains Experimental Range (Colorado, USA).

Figure 6

Observed (left array) versus simulated (right array) tree size distributions (histograms, left scale) and size dependent growth rate (line chart, right scale). DBH class definitions are in 5-cm intervals starting from 5 cm (i.e., 5–10 cm, 10–15 cm, ... , and above 50 cm). For the each simulation site, only one woody PFT that corresponded with the dominant trees of the observation site was allowed to establish; (a) Shiretoko site for BoNE, (b) HBEF site for BoBS, (c) Ogawa site for TeBS, (d) Yakushima site for TeBE, and (e) Serimbu site for TrBE. Descriptions of these sites are shown in Table 2.

Figure 7

Simulated changes in LAI after fire, simulated in three forested sites.

Figure 8

Simulated changes in the carbon pool after fire, simulated in three forested sites.

Figure 9

Simulated changes in carbon fluxes after fire, simulated in three forested sites.

Figure 10

Simulated water flux; seasonal changes at 200 yrs after fire, simulated in three forested sites and a grassland site.

Figure 11

Simulated changes in physiognomy during 500 years at the Yakushima site. Yellow trees are temperate needle-leaved evergreens (TeNE), dark green trees are temperate broad-leaved evergreen trees (TeBE), and light green trees are temperate broad-leaved summergreen trees (TeBS). Grass PFTs are not represented. All experiments share identical environmental conditions, although spin-ups were conducted under cooler conditions in experiment 1 and 3, drier conditions in experiment 2 and 4. For distributing PAR among individual trees, horizontal structure was ignored for experiment 3 and 4.

Figure 12

Simulated changes in tree biomass during 500 years at the Yakushima site. TeNE, TeBE, and TeBS represents, respectively, temperate needle-leaved evergreen trees, temperate broad-leaved evergreen trees, and temperate broad-leaved summergreen trees. Grass PFTs are not shown. All experiments share identical environmental conditions, although spin-ups were conducted under cooler conditions in experiment 1 and 3, drier conditions in experiment 2 and 4. For distributing PAR among individual trees, horizontal structure was ignored for experiment 3 and 4. Each experiment was repeated for 10 times, and its averaged result was shown.

Figure 13

Comparison of natural vegetation to simulated vegetation. The natural vegetation map is taken from Haxeltine and Prentice (1996) with some simplifications.

Tables

Table 1. Plant Functional Types (PFTs) in the SEIB–DGVM, and their abbreviation

Plant Functional Type	abbreviation
Tropical broad-leaved evergreen	TrBE
Tropical broad-leaved raingreen	TrBR
Temperate needle-leaved evergreen	TeNE
Temperate broad-leaved evergreen	TeBE
Temperate broad-leaved summergreen	TeBS
Boreal needle-leaved evergreen	BoNE
Boreal needle-leaved summergreen	BoNS
Boreal broad-leaved summergreen	BoBS
Temperate herbaceous (C_3 grass)	TeH
Tropical herbaceous (C_4 grass)	TrH

1 Table 2. Forest plots, used for model validationtions

Dominant PFT	Site name	location	Altitude (m)	Mean annual temperature (°C)	Annual precipitation (mm)	Plot area (ha)	Interval for growth analysis (years)	Data source
BoNE	Shiretoko (Japan)	43°59' N, 145°1' E	500	2.6	1300	1.25	6	PlotNet
BoBS	HBEF (USA)	43°56' N, 71°45' W	650	6.8	1400	9.96	10	Hubbard Brook Ecosystem Study
TeBS	Ogawa (Japan)	36°56' N, 140°35' E	640	14.2	1401	6.00	6	FFPRI (2003)
TeBE	Yakushima (Japan)	30°20' N, 130°24' E	650	16.4	3230	0.44	5	PlotNet
TrBE	Serimbu (Indonesia)	0°45' N, 110°06' E	N.A.	N.A.	4300	2.00	3	PlotNet

2

Figure01 (Adobe-Illustrator file)

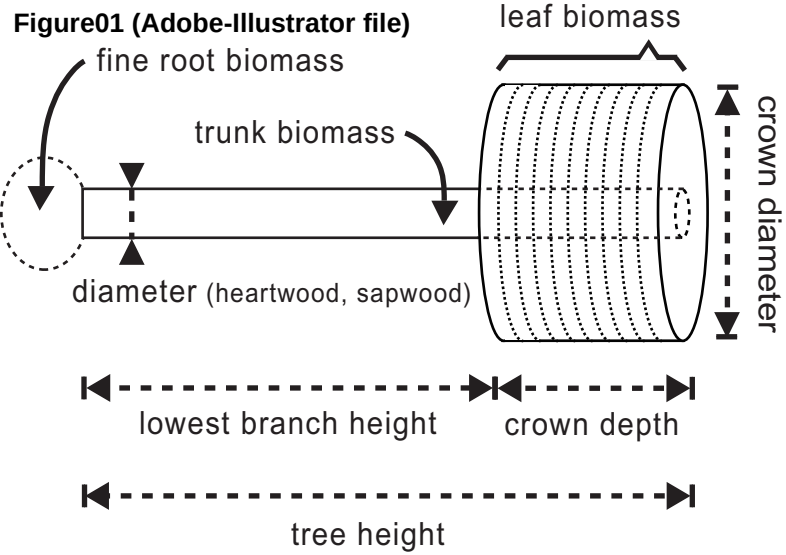

Figure02 (Adobe-Illustrator file)

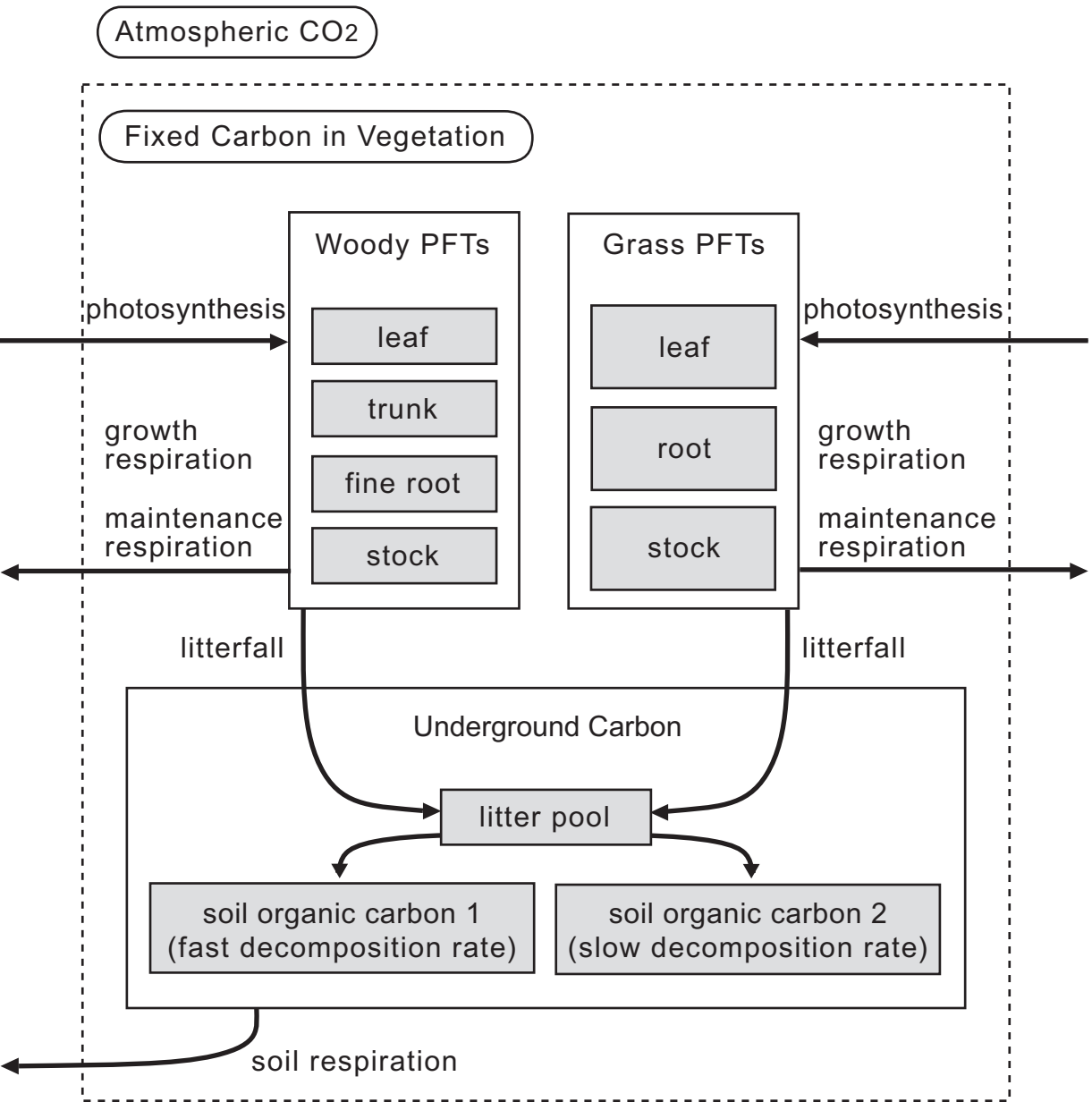

Figure03 (Adobe-Illustrator file)

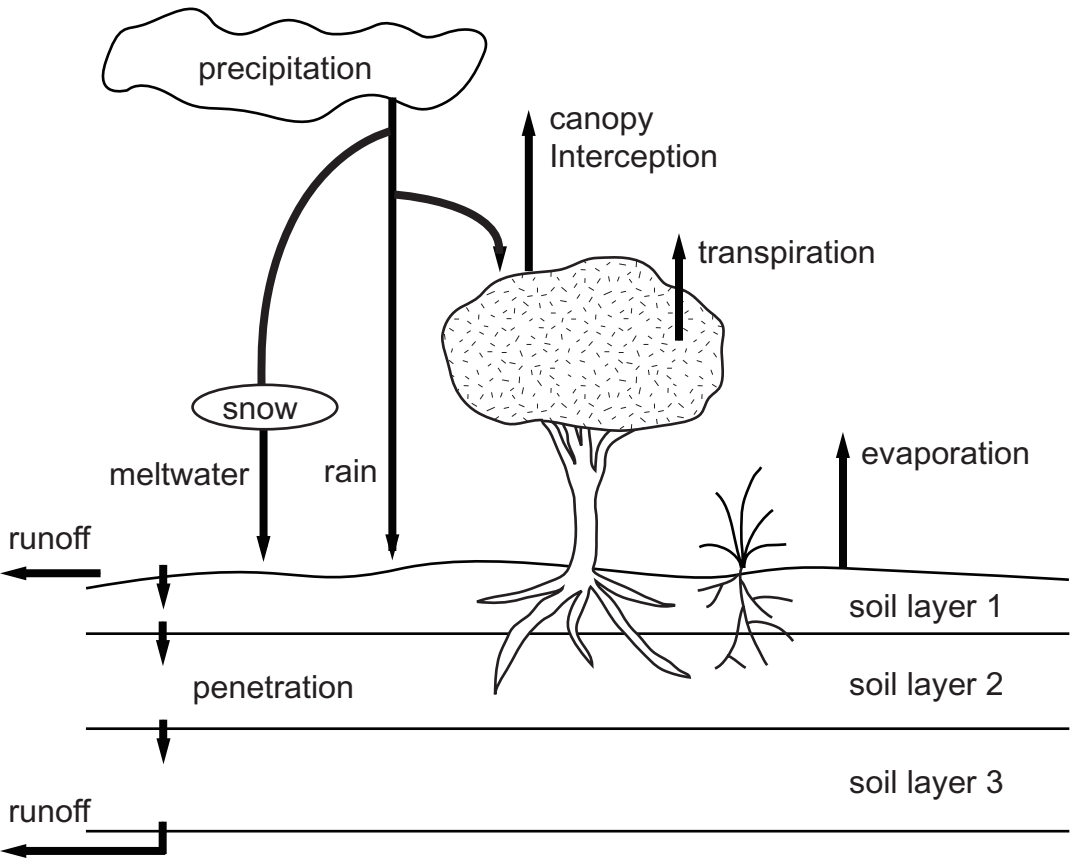

Figure04 (Adobe-Illustrator file)

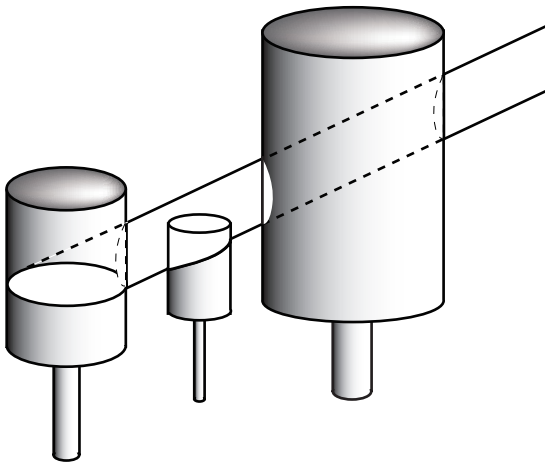

Figure05 (Adobe-Illustrator file)

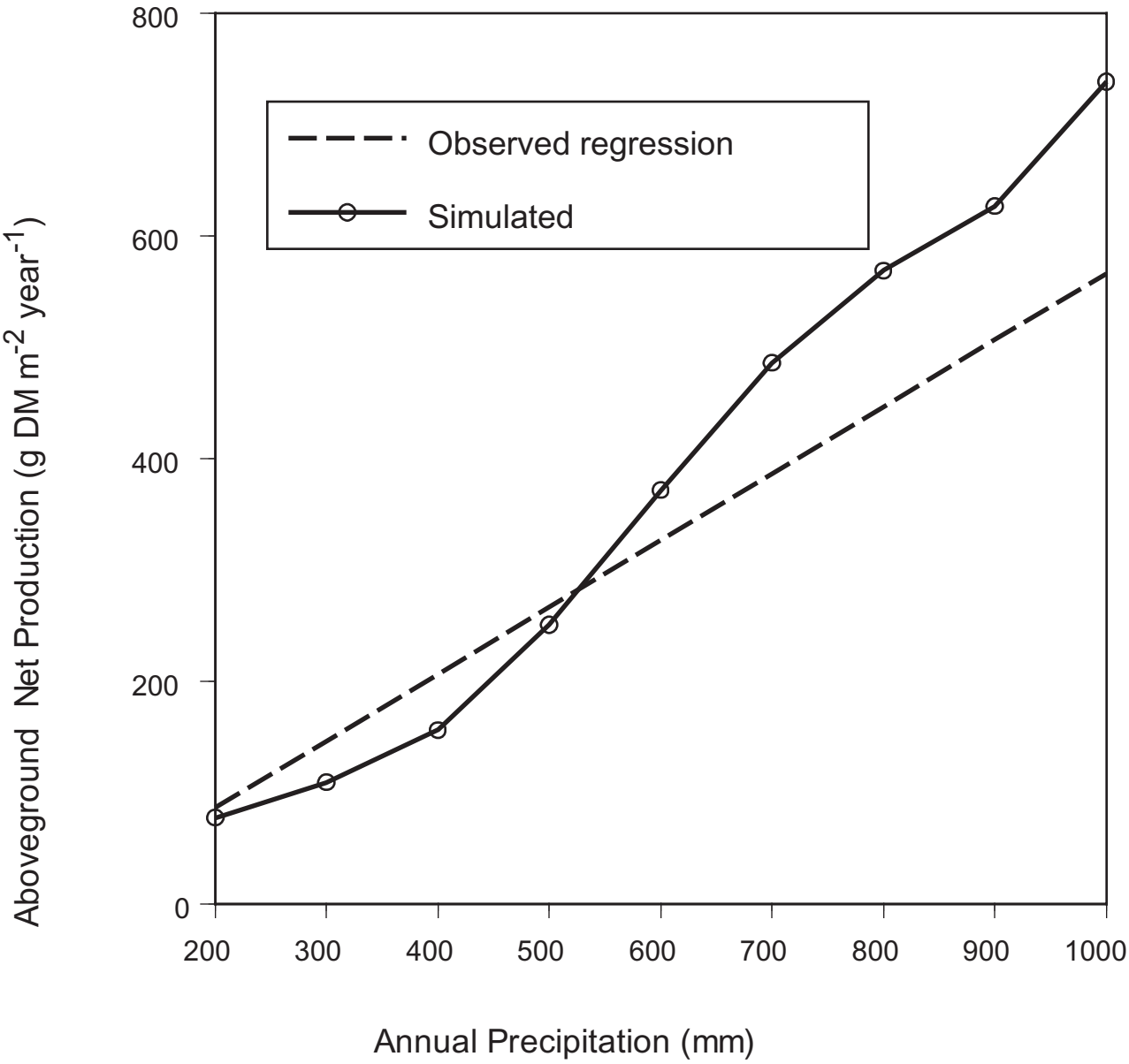

Figure06 (Adobe-Illustrator file)

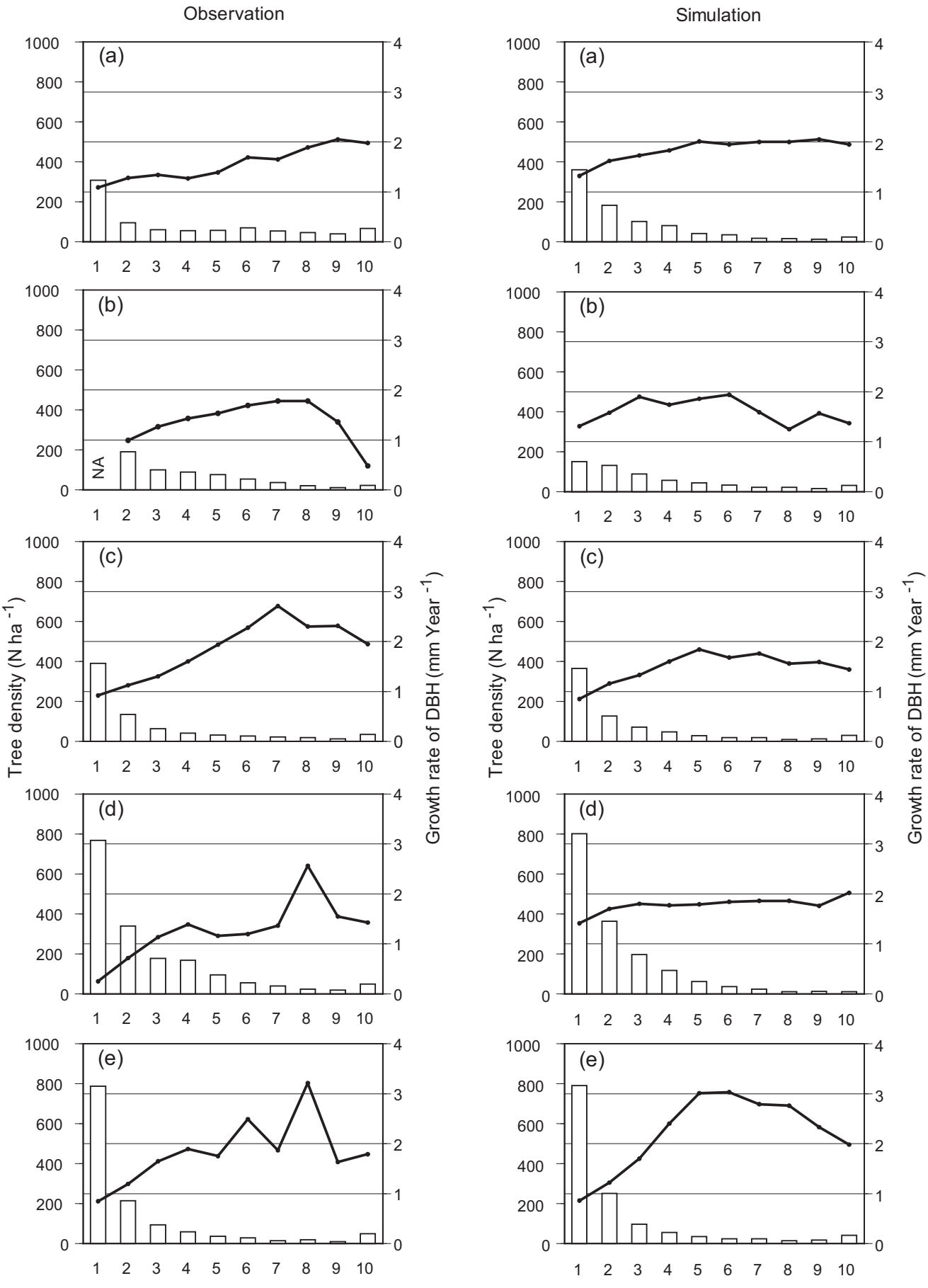

Figure07 (Adobe-Illustrator file)

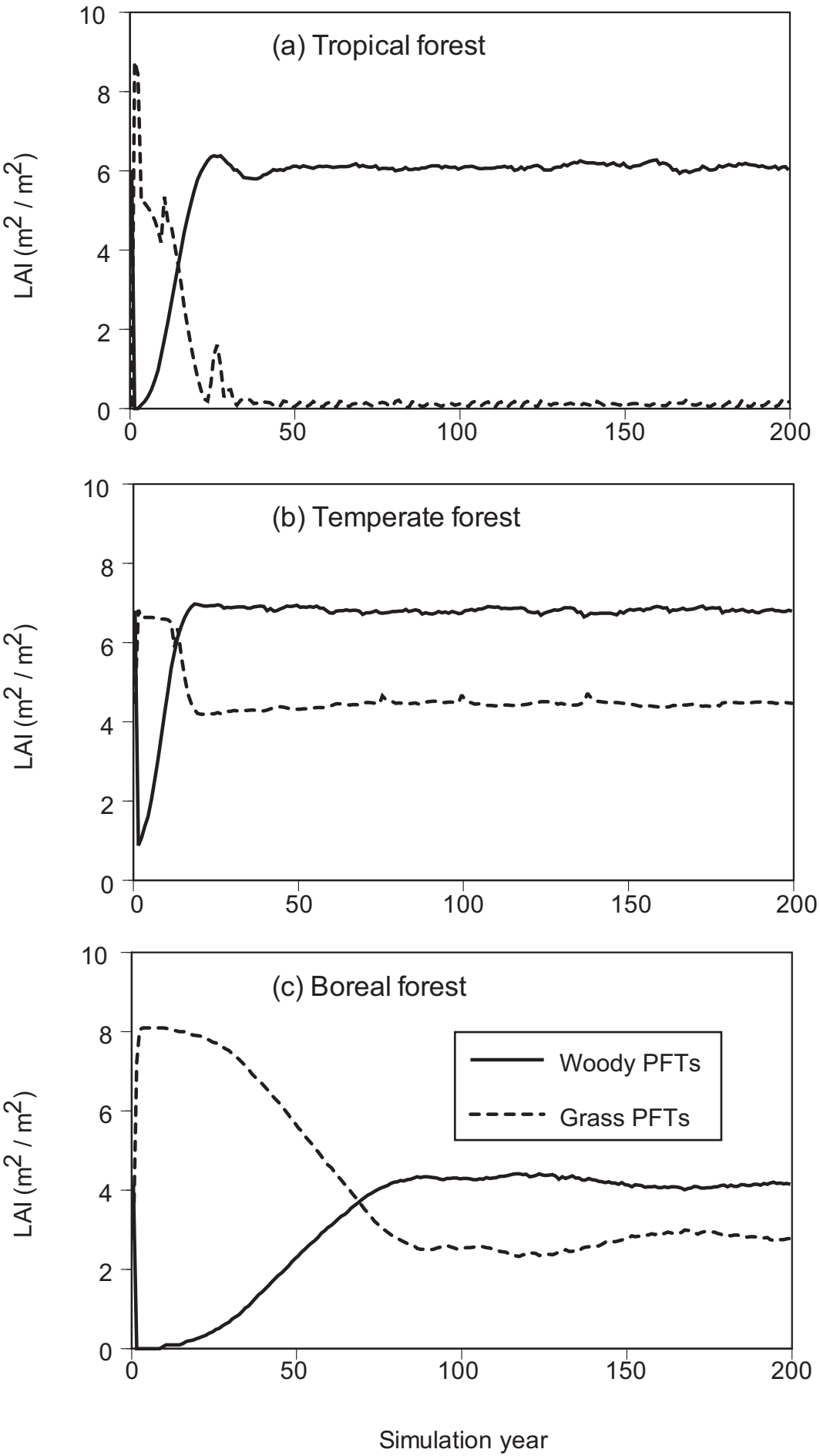

Figure08 (Adobe-Illustrator file)

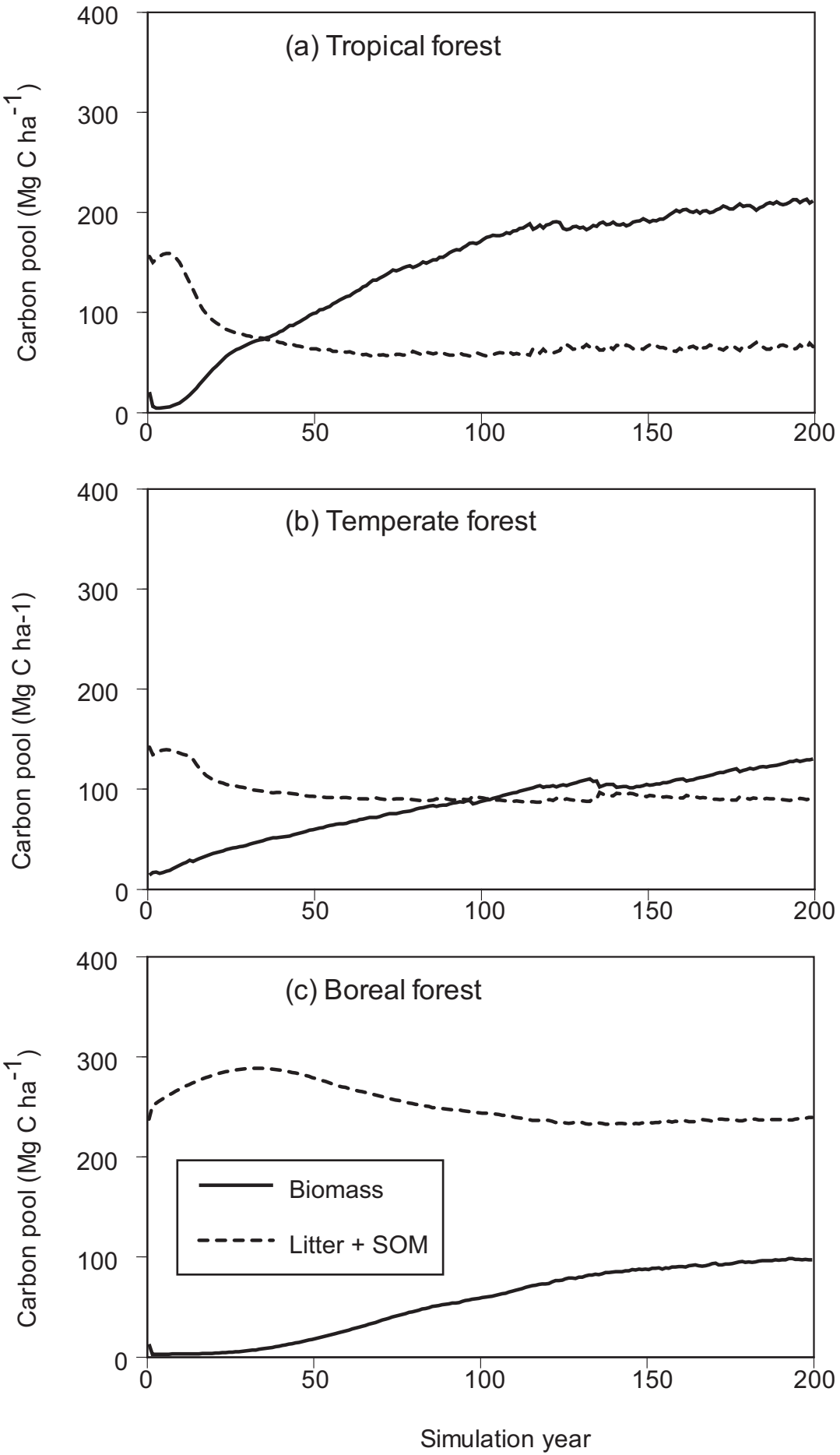

Figure09 (Adobe-Illustrator file)

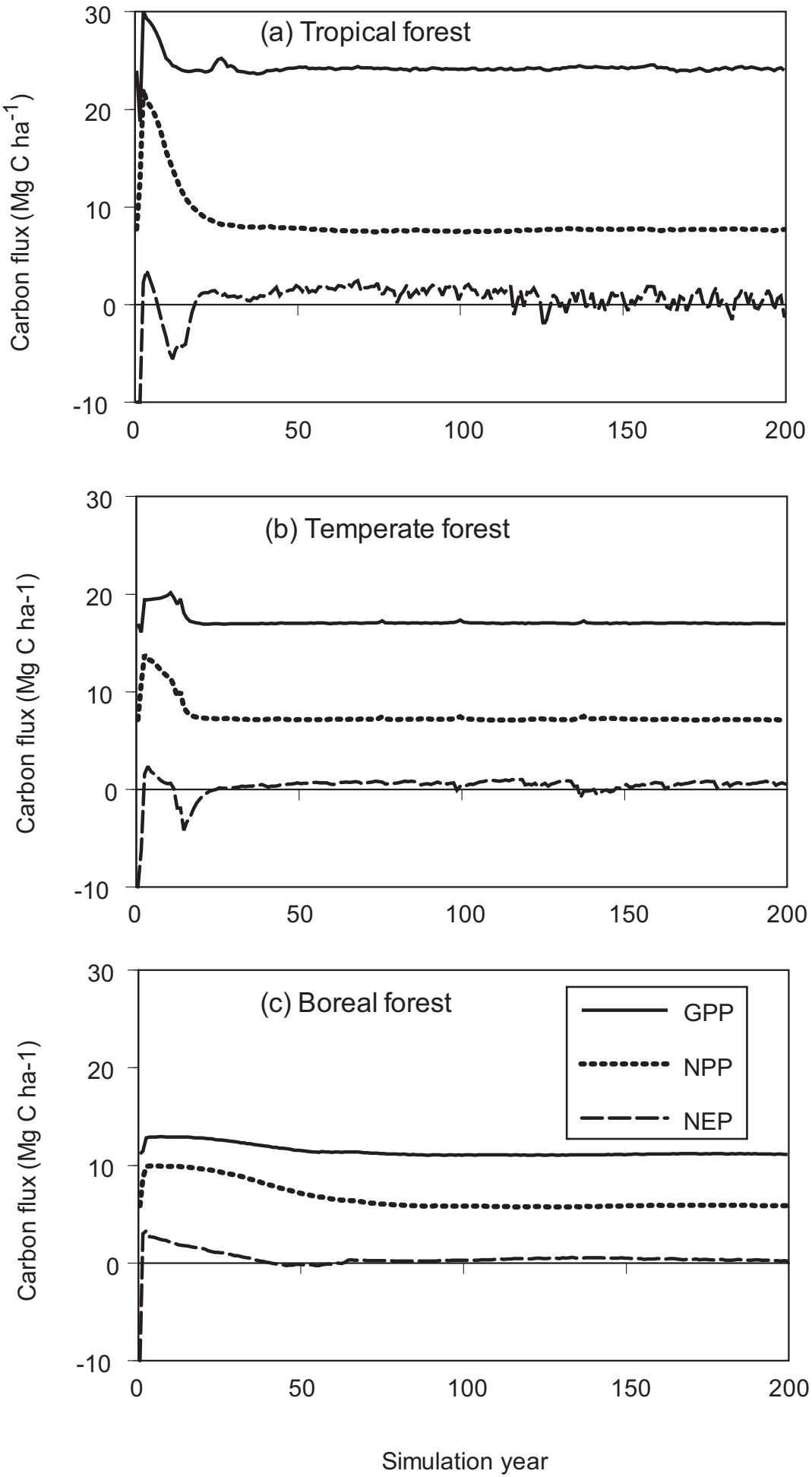

Figure10 (Adobe-Illustrator file)

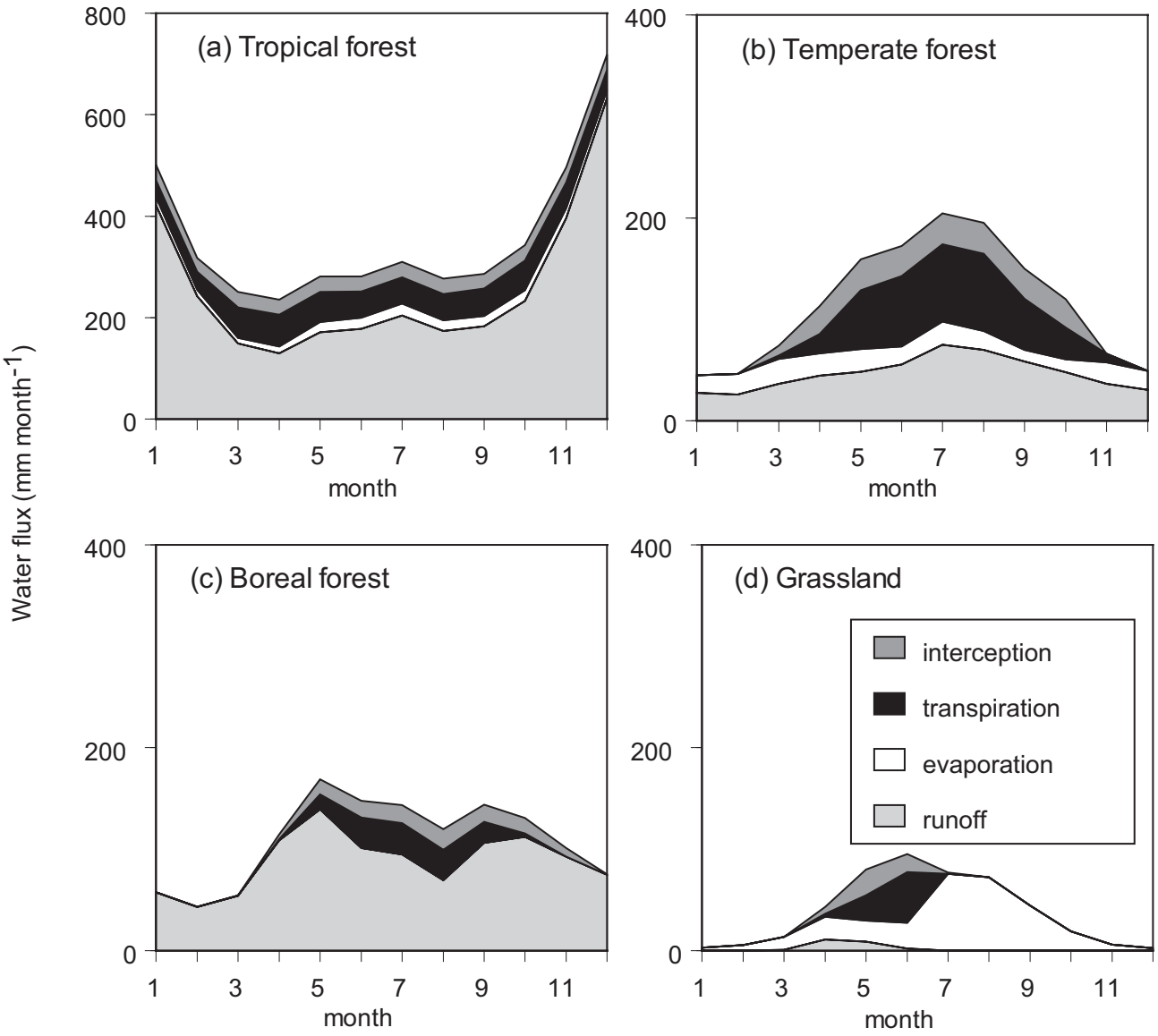

Figure11 (Adobe-Illustrator file)

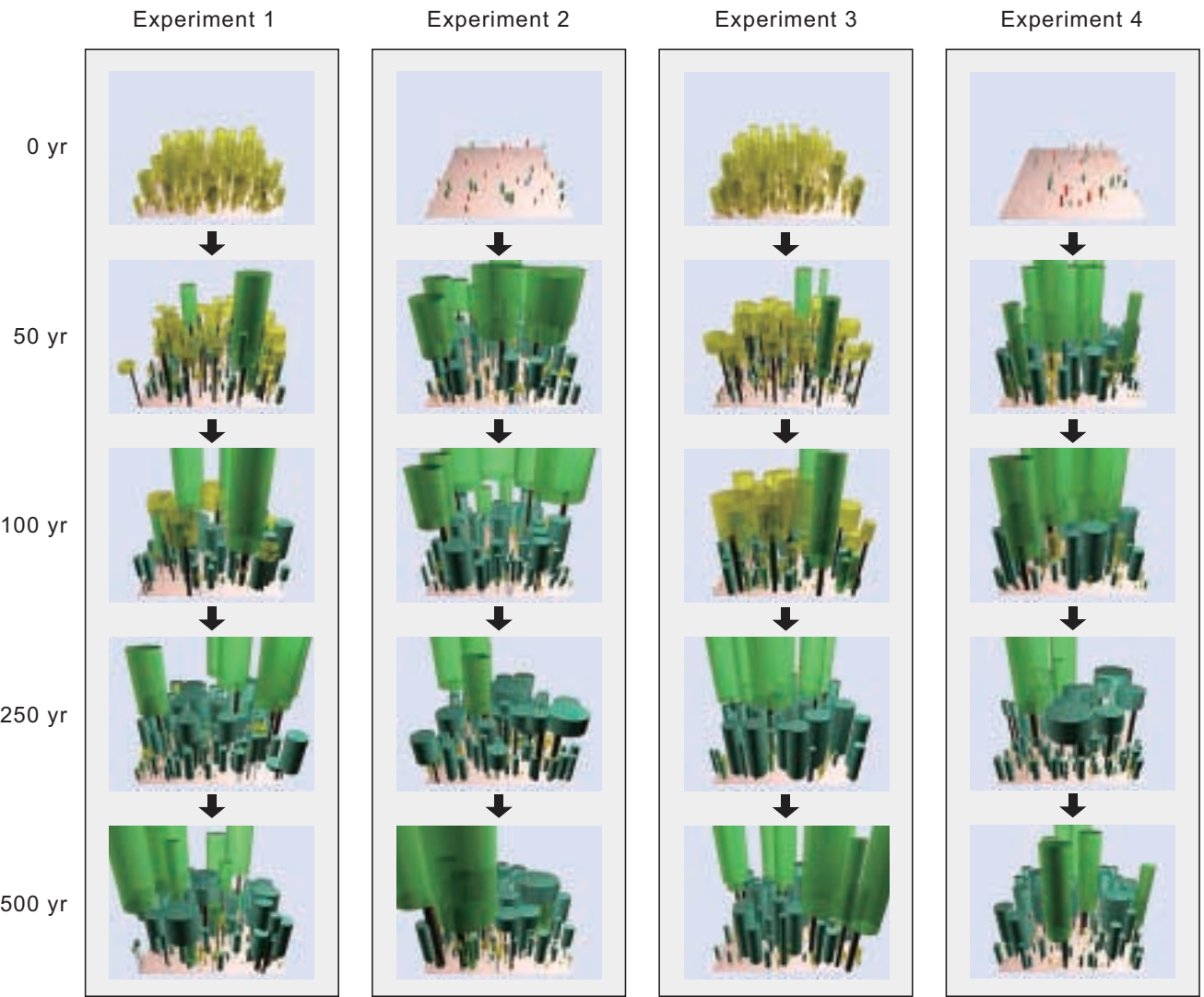

Figure12 (Adobe-Illustrator file)

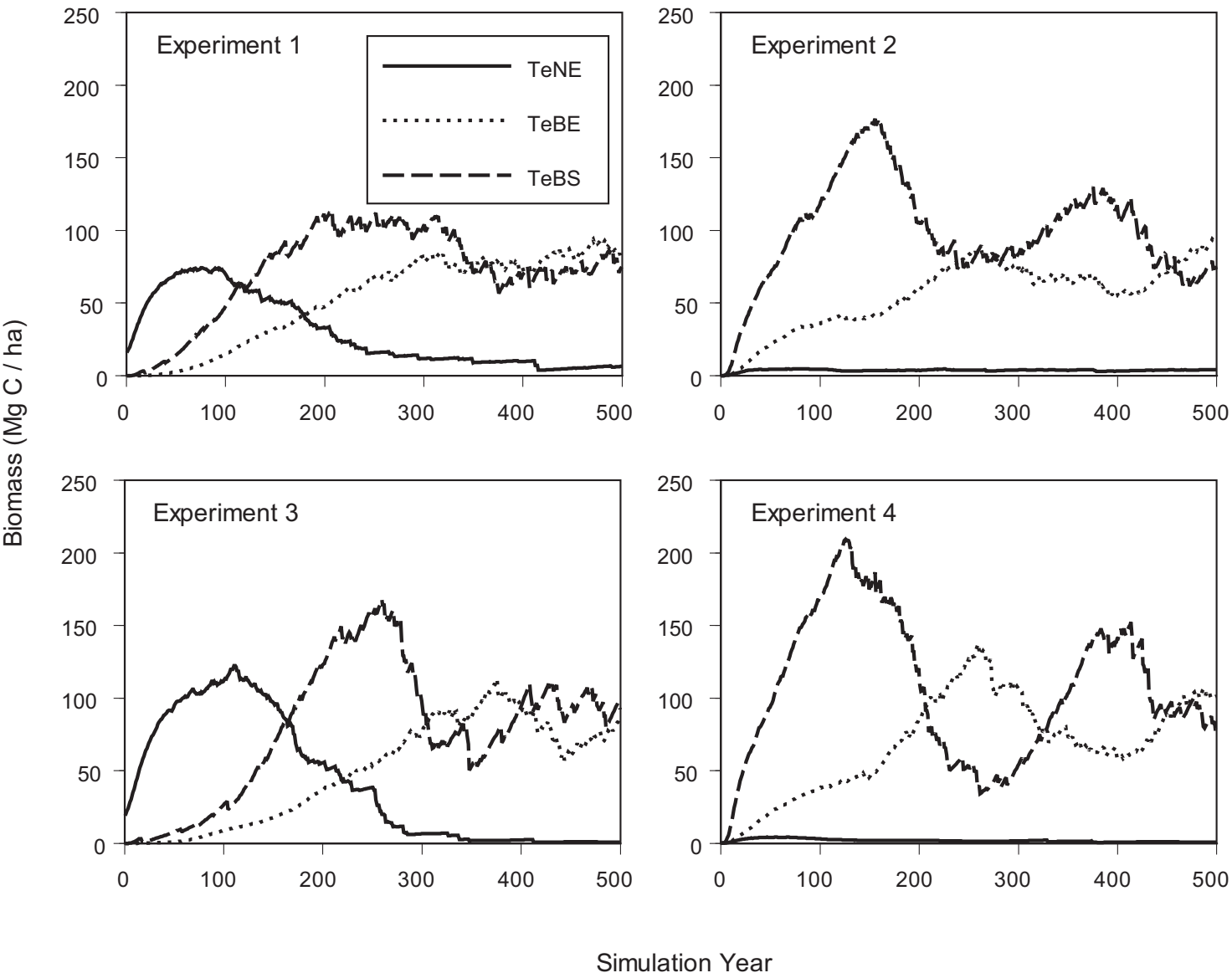

Figure13 (Adobe-Illustrator file)

Natural vegetation

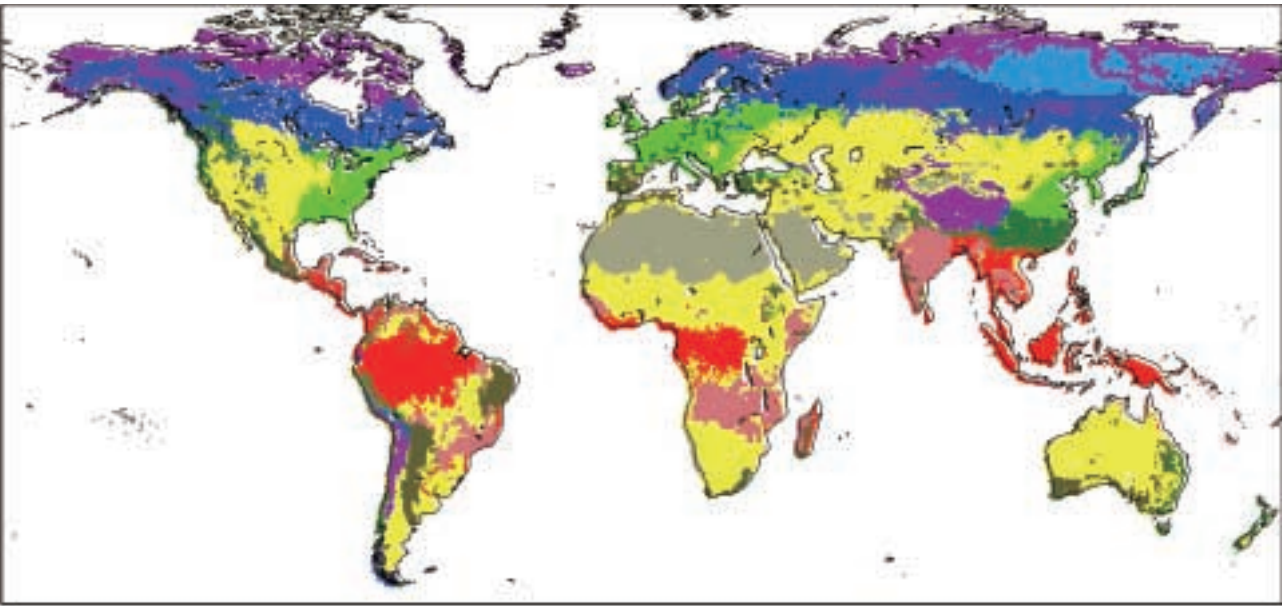

Simulated vegetation